Geology and geochronology of the Two-Thirty Prospect, Northparkes district, NSW

T. J. Wells[a]*, David R. Cooke[a,b], M. J. Baker[a,b], L. Zhang[a,b], S. Meffre[a], J. Steadman[a] , M. D. Norman[c] and J. L. Hoye[d]

[a] Centre for Ore Deposit and Earth Sciences, CODES – University of Tasmania, Private Bag 79, Hobart, Tas 7001, Australia; [b]ARC Industrial Transformation Research Hub for Transforming the Mining Value Chain – TMVC, University of Tasmania, Private Bag 79, Hobart, Tas 7001, Australia; [c] Research School of Earth Sciences, The Australian National University, ACT 2601, Australia; [d] Northparkes Mines, PO Box 995, Parkes, NSW 2870, Australia

*Corresponding author: Tristan Well email tjwells@utas.edu.au

T. J. Wells https://orcid.org/0000-0001-5229-4619,

David. R. Cooke https://orcid.org/0000-0003-3096-5658.

Michael. J. Baker https://orcid.org/0000-0002-8050-7631,

S. Meffre https://orcid.org/0000-0003-2741-6076,

J. Steadman https://orcid.org/0000-0003-4679-3643

Marc D. Norman https://orcid.org/0000-0002-1357-5415

Received; accepted November 2020

Editorial handling: Anita Andrew

Abstract

The Northparkes district, central New South Wales, hosts several economic Cu–Au deposits associated with discrete, thin, porphyry intrusive complexes emplaced in the Late Ordovician during formation of the Macquarie Arc. The recently discovered Two-Thirty Cu–Au–(Mo) prospect is a mineralised magmatic-hydrothermal breccia complex that is hosted by the moderately east-dipping Goonumbla Volcanic Complex on the western limb of the Milpose syncline ~15 km south of the Northparkes porphyry district. Generation of the magmatic-hydrothermal breccia complex is interpreted to be related to the 448.0 ± 4.4 Ma emplacement of the Two-Thirty porphyry. However, Re–Os dating of molybdenite from the breccia complex indicates a potential for a *ca* 440 Ma mineralising event that has similar timing to economic porphyry mineralisation in the Northparkes district. The discovery of the Two-Thirty prospect has important implications for exploration in the Northparkes district and the broader Macquarie Arc. Two-Thirty is only the second known occurrence of magmatic–hydrothermal breccia-hosted mineralisation discovered within the Macquarie Arc, with the other being Cadia Quarry. Mineralisation at Two-Thirty is potentially older than the Northparkes and Cadia deposits, and younger than the epithermal and calc-alkaline deposits at Cowal, Marsden and Ridgeway.

Key Points:

1. The Two-Thirty is a polyphase magmatic-hydrothermal breccia complex that hosts Cu–Au (Mo).
2. The Two-Thirty is the first significant breccia-hosted mineralisation found in the Northparkes district.
3. U–Pb zircon crystallisation ages of the causative intrusion at Two-Thirty pre-date mineralisation at Northparkes.
4. Re–Os dates of molybdenite from the Two-Thirty breccia complex are coeval with syn-mineralisation at Northparkes, supporting the model of periodic release of melts and fluids from underlying magma chambers during the formation of porphyry mineralisation in the Northparkes district.

Keywords: Macquarie Arc, Northparkes, porphyry, magmatic-hydrothermal breccia, Cu–Au (Mo),

Introduction

The Northparkes district, located ~25 km northwest of Parkes, NSW, contains five economic Cu–Au porphyry deposits (Endeavour [E] 22, 26, 27, 48 and GRP314; Figure 1) and numerous sub-economic prospects (Cooke *et al.*, 2007; Smith *et al.*, 2004). Mineralisation in the Northparkes district is associated with Late Ordovician to earliest Silurian (444 to 439 Ma) alkalic monzonite porphyries (Cooke *et al.*, 2007; Pacey et al., 2019; Wells *et al.*, 2020). The recently discovered Two-Thirty intrusive complex prospect to the southwest of the Northparkes district is the focus of this study.

The Two-Thirty prospect is a mineralised magmatic-hydrothermal breccia complex associated with Middle to Late Ordovician *ca* 455 to 439 Ma monzonitic porphyries hosted by the 455–444 Ma Goonumbla Volcanics. Significant mineralised intercepts from the Two-Thirty (Table 1) occur predominantly at depth and its discovery by Northparkes mines in late 2015 has important implications for understanding the magmatic and hydrothermal history of the Northparkes district. The Two-Thirty prospect is unique in that it is the only known mineralised magmatic-hydrothermal breccia discovered in the Northparkes district and high-grade Au in distal veins at the prospect are commonly associated with Pb, Zn and Te, which suggests that it may be one of only a few significant occurrences of low-intermediate sulfidation associated mineralisation in the district. It is located ~15 km southwest of the cluster of alkalic porphyry deposits (E22, 26, 27, 48 and GRP314) in an area that contains three high-grade Au epithermal and skarn prospects (E6, E7 and E44; B. M. Jones, 1991; G. J. Jones, 1985; Lickfold *et al.*, 2007). This study documents the geology, alteration, mineralisation, and geochronology of Two-Thirty, and discusses some key aspects of the timing of the Two-Thirty magmatism and mineralisation in the context of the Macquarie arc.

Geological setting

The Macquarie Arc is an Ordovician oceanic island arc that was accreted to the Australian mainland during the Late Ordovician to early Silurian Benambran Orogeny (Crawford *et al.*, 2007a). Basement to the Macquarie Arc is inferred to be an earlier Cambrian island arc based on Hf isotope compositions of zircons from Cambrian intrusive rocks (Kemp *et al.*, 2020; Meffre *et al.*, 2018; Zhang *et al.*, 2019). Magmatism that formed the Macquarie Arc commenced prior to 484 Ma (Early Ordovician; Crawford, Glen, *et al.*, 2007; Glen, Crawford, & Cooke, 2007; Percival & Glen, 2007). Four phases of intra-oceanic arc-type magmatism formed the Macquarie Arc (Glen, Crawford, & Cooke, 2007). Each magmatic event was followed by a hiatus in volcanism

during which shallow marine limestone was deposited (Table 2; Crawford, Meffre, *et al.*, 2007; Percival & Glen, 2007). Each phase of magmatism had characteristic magmatic affinities that reflect the evolution of the volcanic arc (Glen, Crawford, & Cooke, 2007). The tectono-magmatic development of the Macquarie Arc continued until the earliest Silurian (438 Ma) when volcanism ceased (Crawford, Meffre, *et al.*, 2007) culminating in alkalic porphyry Cu–Au mineralisation at Cadia (Harris *et al.*, 2014, 2020; Wilson *et al.*, 2003, 2007) and Northparkes (Lickfold *et al.*, 2003, 2007; Pacey *et al.*, 2019; Wells *et al.*, 2020).

The Macquarie Arc today consists of four volcanic belts that have been fault juxtaposed against Ordovician to early Silurian quartz-rich turbidite sequences that dominate the Lachlan Fold Belt (Cooke *et al.*, 2007; Crawford, Glen, *et al.*, 2007; Glen *et al.*, 2009; Zukowski *et al.*, 2014). The three major belts of Ordovician volcanic, volcaniclastic, limestone and intrusive rocks in the Lachlan Fold Belt are the Junee-Narromine, Molong, and Rockley-Gulgong belts (Lickfold *et al.*, 2007; Figure 1). A fourth correlate, the Kiandra Belt, is exposed to the southeast in the Snowy Mountains (Crawford, Glen, *et al.*, 2007; Glen, Crawford, & Cooke, 2007). Economically significant mineralisation has been discovered in the Molong and Junee-Narromine belts. The Junee-Narromine Belt, which is the most geologically diverse belt in the Macquarie Arc, is subdivided into a series of igneous and volcanic complexes including the Goonumbla Volcanic Complex that hosts the Northparkes porphyry deposits as well as the Two-Thirty prospect (Table 3; Lickfold *et al.*, 2003, 2007).

Goonumbla Volcanic Complex

The Nelungaloo Volcanics are the basal Early Ordovician unit of the Goonumbla Volcanic Complex (Glen, Crawford, Percival, *et al.*, 2007; Glen, Spencer, *et al.*, 2007; Percival & Glen, 2007). The thickness of the unit is estimated to be ~600 m assuming no structural repetition (Krynen *et al.*, 1990). Volumetrically minor, unmineralised monzodiorite porphyries intruded the Nelungaloo Volcanics at 481± 4 Ma (Glen, Spencer, *et al.*, 2007; Simpson *et al.*, 2005).

The Goonumbla Volcanics overlie the Nelungaloo Volcanics on a low-angle unconformity (Krynen *et al.*, 1990; Lickfold *et al.*, 2007). The basal unit of the Goonumbla Volcanics is a volumetrically minor basaltic andesite lava. A trachyandesitic lava that varies from massive to auto-brecciated overlies the basal unit (Simpson *et al.*, 2005). The bulk of the Goonumbla Volcanics are composed of similar trachyandesitic lavas and associated volcaniclastic conglomerates (Lickfold, 2002; Simpson *et al.*, 2005). Monzodiorite intrusions in the Goonumbla Volcanics are differentiated from the Nelungaloo monzodiorite intrusions by a higher proportion of interstitial alkali feldspars (Crawford, 2001).

The intermediate to felsic Wombin Volcanics conformably overlie the Goonumbla Volcanics (Krynen *et al.*, 1990). Simpson *et al.* (2005) interpreted the presence of ignimbrites and trachyte lavas in the Wombin Volcanics to indicate voluminous subaerial to subaqueous explosive eruptions and sector collapse of volcanic edifices. Numerous monzonite and quartz monzonites intruded the Wombin Volcanics, including quartz monzonite porphyry (QMP) pipes associated with the Endeavour 22, 26, 27 48 and GRP314 deposits (Lickfold *et al.*, 2007; Pacey *et al.*, 2019; Wells *et al.*, 2020).

Magmatism in the Northparkes district

The intrusive history of the Northparkes district is complex, with multiple generations of monzonitic porphyries emplaced in the Late Ordovician exhibiting only subtle variations in mineralogy and texture (Table 4). Detailed logging and petrographic analysis of the Northparkes intrusive complex at E22, 26, 27 and 48 detailed at least eight intrusive phases (Lickfold, 2002; Lickfold *et al.*, 2003, 2007; Pacey *et al.*, 2019).

The Northparkes porphyry deposits are localised on a narrow, ~4 km-long northwest-trending linear structure that is inferred from geomagnetic data (Heithersay & Walshe, 1995; Heithersay *et al.*, 1990; Lickfold *et al.*, 2003; Figure 2). At deposit scale, the northwest- and northeast-trending quartz sulfide veins define the main vein stockwork (Harris & Holcombe, 2014).

Mineralisation in the Macquarie Arc

The Macquarie Arc contains alkalic and calc-alkalic porphyry, high sulfidation Au (± Cu), Au–Cu–Fe skarn and alkalic intermediate sulfidation carbonate–base-metal epithermal deposits (Cooke *et al.*, 2007; Supplementary Table 1). These are similar in style to the deposit types observed in Cenozoic oceanic island arc settings (e.g., Papua New Guinea, Philippines, Indonesia; Cooke *et al.*, 2007; Fox *et al.*, 2015; Glen *et al.*, 2012; Harrison *et al.*, 2018; Rinne *et al.*, 2018; Sykora, Selley, *et al.*, 2018).

High-grade porphyry Cu–Au mineralisation at Northparkes was genetically related to small volume, oxidised and evolved shoshonitic magmas, localised by transverse structures in the Macquarie Arc (Glen *et al.*, 2012; Phase 4 porphyries, Table 2; Glen, Crawford, & Cooke, 2007; Lickfold, 2002). Mineralisation at Northparkes produced bornite, chalcopyrite and gold (free and refractory), which occur as infill in quartz–sulfide ± magnetite ± carbonate stockwork veins and minor breccias (Cooke *et al.*, 2007). Unidirectional solidification textures, and miarolitic cavities intimately link volatile exsolution during intrusive activity, with mineralisation at Northparkes (Cooke *et al.*, 2007; Lickfold, 2002).

Methods

Description of lithology, alteration, veins, and breccias

The method for identifying intrusive phases at Two-Thirty was adopted from the petrography-based scheme developed for Northparkes by Lickfold *et al.* (2003, 2007). Intrusive phases were classified based on five textural characteristics: (1) phenocryst abundance; (2) nature of groundmass; (3) total proportions of mafic phenocrysts; (4) proportion of non-mafic phenocrysts; and (5) presence or absence of primary anhedral to euhedral, composite or single quartz grains within the groundmass. Classification of each intrusive phase was based on primary quartz, plagioclase and alkali-feldspar content in accordance with the IUGS nomenclature proposed by Streckeisen (1976).

Veins and altered rocks were logged using a modified version of the Anaconda method adapted for drill core (Blackwell, 2010; Einaudi, 1997). The alteration, vein and breccia paragenesis were determined from observations of crosscutting and overprinting relationships. Each event was assigned a pre-, syn- or post-brecciation timing. Alteration mineral identification was supplemented using shortwave wave infrared (SWIR) analyses on rock samples.

Breccia facies analysis was carried out based on the framework outlined by Davies (2002), with nomenclature and description of breccia facies based on Davies (2002), McPhie *et al.* (1993) and Mort and Woodcock (2008). Internal variations in the breccia complex necessitated the subdivision of breccias into subfacies, based on mineralogy of cement, clast composition, shape and angularity as well as the abundance of clasts and cement (Supplementary Table 2).

Geochronology

Zircons

Five igneous phases of the Two-Thirty intrusive complex were selected for U–Pb zircon geochronology at the CODES Analytical Laboratories at the University of Tasmania. A total of 200 to 400 g of each sample was milled in a Cr-steel ring mill and sieved to exclude grains >400

μm. Separation of the fine fraction involved panning and magnetic separation. Samples with extensive pyrite were baked at 450°C to oxidise pyrite to pyrrhotite, which was then removed by further magnetic separation. Zircon grains were handpicked for mounting using cross-polarised transmitted light microscopy. Targeting of suitable grains was facilitated by cathodoluminescence imaging using the FEI MLA 650 environmental scanning electron microscope at the University of Tasmania Central Science Laboratory.

The data were obtained by laser ablation inductively coupled plasma mass spectrometry (LA-ICPMS) analyses. The analytical session employed a 32 μm spot diameter at 10 Hz. Data reduction included the manual screening of analyses to identify zircons that were (1) substantially older than the main population, indicating the presence inherited cores or xenocrysts, or (2) had high levels of U and Pb loss as a result of radiation damage. Zircon spot analyses that intersected high Pb inclusions were also discarded from final age calculations. Samples with a small amount of common Pb were corrected using the ^{207}Pb method (Tera & Wasserburg, 1972), with the composition of the common Pb calculated using the model of Stacey and Kramers (1975). Results were plotted using the Isoplot extension in Microsoft Excel (Berkley Geochronology Center, 2015).

Molybdenite

Re–Os dating of molybdenite (Stein *et al.*, 2001) was conducted on one sample from the Two-Thirty breccia complex and one sample each from the Northparkes E27 and E48 deposits. The samples were analysed at RSES-ANU using methods described by Armistead *et al.* (2017), Kemp *et al.* (2020) and Norman *et al.* (2004).

Briefly, molybdenite was separated from the bulk sample using heavy liquid separation and handpicking to obtain a visually pure separate. These separates were weighed, spiked with precisely calibrated solutions of ^{185}Re and common Os , and digested in Carius tubes (Shirey & Walker, 1995) using inverse aqua regia (HNO_3–HCl) at 250ºC for 12 hrs. Following digestion of the sample, Re and ^{187}Os concentrations were determined by isotope dilution mass spectrometry using a Neptune magnetic sector multi-collector ICPMS. For the Os analyses, the volatile OsO_4 was purged from the sample solution directly into the multi-collector ICPMS using the Ar carrier gas. Rhenium isotopic compositions were measured separately by solution aspiration after separation of the Re by anion exchange chromatography. An uncertainty of ± 0.5% was assigned to the ages based on the long-term reproducibility of the HLP-5 reference molybdenite analysed in this laboratory (Kemp *et al.*, 2020).

LA-ICPMS element mapping

LA-ICPMS mapping of the distribution of Re contents within individual molybdenite grains from E48 and E27 at Northparkes and from the A3 breccia facies at Two-Thrity were carried out at CODES, University of Tasmania, using an Agilent 7500 ICPMS coupled to a Resolution S155 Laser ablation cell and an ATL 193 nm excimer ArF laser. Images were obtained by ablating a sequence of parallel lines with no spacing between them (Danyushevsky *et al.*, 2011; Gregory *et al.*, 2013; Large *et al.*, 2009). Beam size ranged between 10 and 22 μm depending on the size of the grain of interest. A pre-ablation pass was made over each line to remove surface contamination from the previous ablation pass (Sykora, Cooke, *et al.*, 2018). The rastering speed of the beam across the sample at a rate equal to the beam size (i.e. 10 μm beam at 10 μm/s) with a laser frequency of 10 Hz and an energy density of ~3 Jcm^{-2}. Spot analysis of external standards (STDGL2b2, BCR-2G and GSD-1G) were conducted prior to and following each image to correct instrumental drift (Danyushevsky *et al.*, 2011; Hnatyshin *et al.*, 2020).

Conversion from counts per second (CPS) to concentration (ppm) was undertaken using in house software, using calculations based on previous publications from CODES, University of

Tasmania (e.g., Steadman *et al.*, 2015; Sykora, Cooke, *et al.*, 2018). Concentration data were subsequently plotted using a sequential, perceptually uniform colour palette that removes some of the visual bias of traditional logarithmic rainbow colour stretches (Robertson & Callaghan, 1988; Smith & van der Walt, 2015).

Observations

Geology of the Two-Thirty Prospect

The Two-Thirty Cu–Au (Mo) prospect is hosted by moderately east-dipping Goonumbla Volcanics on the western limb of the Milpose syncline (Figure 2). Here, the Goonumbla Volcanics consist of a lower sequence of moderate to poorly sorted polymictic volcaniclastic breccias, which commonly contain imbricated clasts that grade upwards to a series of trachyandesitic sandstones and siltstones. Latite lavas and discontinuous limestone lenses are interbedded with the volcano-sedimentary rocks. Peperitic breccias on some upper latite lava contacts support a subaqueous depositional environment (e.g., McPhie *et al.*, 1993). Subaqueous deposition is further supported by the presence of imbricate clasts within the volcaniclastic breccias, soft-sediment deformation within some fine-grained sedimentary rocks, and local limestone lenses that have been interpreted as slabs of reef facies redeposited during mass flow (Simpson *et al.*, 2005). The Goonumbla Volcanics at the Two-Thirty prospect are interpreted to have been deposited in a shallow to transitional submarine environment proximal to an emergent Middle Ordovician volcano. The interpretation is based on the upward fining turbidite-like sequences with imbricated clasts suggesting deposition by mass flow. Proximity to the volcanic edifice is based on the angularity of grains in the volcaniclastic rocks. Breccias are locally moderately sorted suggesting progressive waning of energy during deposition of the individual beds (McPhie *et al.*, 1993).

The Goonumbla Volcanics were cut by the Two-Thirty intrusive complex, which is composed of ten intrusive phases (Figure 3), including six monzonite–quartz-monzonite porphyries, three of which have textural and mineralogical similarities to porphyry intrusions in the Northparkes Intrusive Complex (Table 4). Intrusive contacts in the Two-Thirty complex have only been observed between a few intrusive phases due to sparse drilling coverage (Figure 4). The intrusions are divided into pre-, syn-, and post-mineralisation groups based on relative timing relationships with respect to mineralisation and alteration.

Pre-mineralisation intrusions

Hornblende–biotite, K-feldspar-phyric quartz monzonite porphyry (KHB-QMP)

The KHB-QMP varies from sparsely feldspar phyric to crystal crowded. Phenocryst phases are ~70 vol% plagioclase and ~30 vol% alkali-feldspar, variable (up to 5 vol%) hornblende and biotite, and minor (3 vol%) and magnetite ± leucoxene. The KHB-QMP has a fine-grained to granular groundmass with rare quartz crystals. K-feldspar phenocrysts are variably megacrystic (up to 3 cm). The abundance of hornblende phenocrysts, lack of clots of chalcopyrite, pyrite or anhydrite and less intense hydrothermal alteration are the distinguishing features of the KHB-QMP.

Alteration of the KHB-QMP is dominated by weak muscovite–phengite alteration of feldspars and minor, selective chlorite alteration of mafic phenocrysts. Selective albite alteration is observed in plagioclase phenocrysts in short intervals of the KHB-QMP. The KHB-QMP typically has fine-grained margins where it intruded sedimentary rocks of the Goonumbla volcanics. Timing of emplacement of the KHB-QMP is inferred to be early based on the presence of (1) partially resorbed mafic xenoliths (Figure 5a), (2) a clast of KHB-QMP occurs in the Two-Thirty porphyry (Figure 5b), and (3) clasts of KHB-QMP occur within the Two-Thirty breccia complex.

Mafic intrusions

Evidence of pre-mineralisation mafic intrusions is limited to small enclaves in a quartz monzonite (KHB-QMP) at 762 m in drill hole D245 (Figure 5a). Complex geometries of the enclaves are interpreted as evidence of partial resorption, and disaggregation of a mafic intrusion within a semi-crystalline monzonite suggesting a subsyngenetic relationship between pre-mineralisation dykes and the KHB-QMP.

Biotite quartz monzonite (BQM) is texturally variable from sparely crystalline to equigranular crystal crowded, with plagioclase, K-feldspar, and biotite phenocrysts and subordinate (<5%) anhedral quartz phenocrysts in an aphanitic to aplitic groundmass (Figure 6a). Veins and xenoliths are rare in this unit. The BQM is variably altered, with chlorite–sericite alteration locally altering mafic phenocrysts. Colour of the BQM varies with alteration intensity from pale pink due to microcrystalline hematite dusting of feldspars to yellow-grey related to phyllic alteration assemblages overprinting the hematite dusting. Clasts of the BQM within the Two-Thirty breccia complex indicate a pre-mineralisation timing for the BQM at Two-Thirty.

Syn-mineralisation porphyries

K-feldspar phyric quartz monzonite porphyry (K-QMP)

This unit is texturally variable from equigranular to weakly porphyritic. Phenocrysts of plagioclase and K-feldspar + minor magnetite and biotite ± hornblende are set in an aphanitic to aplitic groundmass of alkali-feldspar and quartz (Figure 6b). Megacrysts of K-feldspar are a characteristic feature of the K-QMP, as are rare clots of chalcopyrite–pyrite and anhydrite (Figure 6c). Pyrite and chalcopyrite also occur as disseminations, and locally as inclusions in, or as rims around mafic phenocrysts.

Alteration is variable in the K-QMP but is dominated by submicron hematite that instils a pale pink–red colour to the feldspar phenocrysts and groundmass. Selective sericite alteration of feldspar phenocrysts and chlorite alteration of mafic phases are associated with hematite dusting. Strong phyllic alteration (quartz–muscovite–pyrite) occurs locally as an overprint, bleaching the rock pale yellow. The occurrence of sulfide disseminations and inclusions, and the style of alteration is consistent with a syn-mineralisation origin of this unit.

Two-Thirty porphyry

Brecciation and some mineralisation at Two-Thirty is interpreted to be associated with a brick red, moderately crystal crowded, feldspar phyric, monzonite porphyry (Figure 6d). The Two-Thirty porphyry is composed of euhedral K-feldspar and plagioclase phenocrysts with minor, hornblende and clinopyroxene (~5%), biotite ± magnetite and leucoxene (< 1%) in a fine crystalline groundmass of feldspar. Subhedral K-feldspar typically rims euhedral plagioclase phenocrysts.

Alteration is relatively consistent within the Two-Thirty porphyry, with pervasive potassic alteration and hematite dusting. Selective sericite alteration of plagioclase and chlorite after mafic phases occurs as an overprint on the potassic assemblage. Mineralisation consists of disseminations, and veinlets that widen into a breccia cement of pyrite and chalcopyrite, with sparse local disseminations of fine-grained molybdenite.

A ~6 cm diameter xenolith of crystal-crowded megacrystic KHB-QMP occurs in a 9 m interval of the Two-Thirty porphyry (Figure 5b). Xenoliths of volcaniclastic sandstones are present immediately beneath the upper contact of Two-Thirty porphyry. A ~4 mm wide vein of blocky euhedral K-feldspar, conspicuously similar to the cement in the proximal hydrothermal cemented breccia emanates from the upper 30 cm of the Two-Thirty porphyry (Figures 6e and

8c) and is one of the key lines of evidence for the paragenetic relationship between the Two-thirty porphyry and the Two-thirty breccia.

Late mineralisation monzonite porphyry

This intrusion has plagioclase, K-feldspar and minor mafic phenocrysts in a granular plagioclase, K-feldspar groundmass. Mafic phases are altered to biotite and chlorite whereas the groundmass is weakly orthoclase altered and hematite dusted with a late phyllic overprint. Mineralisation is limited to minor disseminated molybdenite and pyrite. Minor leucoxene after titanite is characteristic of this unit.

Post-mineralisation intrusions

Zero porphyries

Zero porphyries are crystal-crowded feldspar-phyric monzonites named for their similarities to late-, post-mineralisation, barren monzonite porphyries at the Northparkes intrusive complex as described by Lickfold *et al.* (2003, 2007). Feldspar phenocrysts are generally <1 mm with occasional larger K-feldspar crystals (~2 mm) in a fine to aphanitic pink feldspathic groundmass. Minor mafic phases are generally weakly altered to a green-grey by sericite and chlorite. Two zero porphyry intercepts occur in drill hole D240 (727–728 m and 772.4–813.9 m; Figure 4). Alteration is highly variable between the two intercepts with the shorter of the two intervals (727–728 m) characterised by moderate phyllic alteration with some albitisation of phenocrysts. The longer interval of zero porphyry (772.4–813.9 m) is relatively unaltered, in comparison to the shorter interval with alteration limited to minor hematite dusting and carbonate veining (Figure 6f).

Aphanitic mafic dykes

Aphanitic mafic dykes are evident in drill hole D240 at 109 m and 132 m with a width of 1–1.5 m. Both dykes have unambiguous intrusive contacts and are weakly sericite altered with minor carbonate veins. A third dyke cross cuts the volcaniclastic sandstones at 704 m in drill hole D247 proximal to a fault.

Aplite dykes and dyklets

Pale, fine-grained aplite dykes with a saccharoidal to aphanitic groundmass of alkali-feldspar with minor biotite. Aplite dykes and dyklets were intersected in drill hole D245 where they crosscut QMP intrusions and sedimentary units. Alteration varies from weak potassic with hematite dusting to pervasive sericite. Most aplite dykes have minor disseminated pyrite and rare carbonate veinlets. However, one interval 552.5m in D245) has abundant disseminated sulfides (pyrite–chalcopyrite) and carbonate base-metal veins (sphalerite, cassiterite and galena), which may be indicative of multiple generations of aplite dykes or a late epithermal mineralisation event.

Pebble dykes

Pebble dykes in the Two-Thirty breccia complex are relatively minor (<20 cm) features. They are matrix-rich with moderate- to well-sorted rounded to ovoid clasts in fine to very fine sand matrix. Provenance of the pebble dykes is interpreted to be the product of steam explosion, creating a milled rock-flour matrix. Clasts are rounded by attrition and abrasion rather than dissolution with the matrix of the breccias made up of comminuted clast material.

Alteration, veins, and breccias

Alteration zonation at the Two-Thirty has been complicated by multiple intrusions, brecciation and overprinting assemblages. A paragenesis has been developed based on overprinting and cross-cutting relationships relative to the main breccia formation (Figure 3).

Stage 1 – pre-breccia hydrothermal alteration

The Goonumbla Volcanics have undergone moderate pervasive biotite–magnetite alteration that is evident in clasts within the Two-Thirty breccia complex (Figure 7a; Table 5). Latite clasts in drill hole D244 have undergone selective quartz + K-feldspar and epidote + chlorite alteration. Stage 1 potassic alteration assemblages are interpreted to indicate that high-temperature potassic and propylitic alteration occurred prior to brecciation (e.g., Corbett & Leach, 1998; Seedorff *et al.*, 2005; Thompson, 1993).

Truncated Stage 1 A, B, and C veins are present in most clast types within the Two-Thirty breccia complex, including Goonumbla Volcanics and juvenile clasts of the Two-Thirty porphyry (Figure 7a). *Stage 1D – sheeted quartz–albite veins* are present in a strongly chlorite–muscovite–altered KHB-QMP at 826.2 (Figure 7b). Similar veins are offset by small-scale faults and stage 3E – carbonate veins in a relatively unaltered KHB-QMP at 848.8 m in D245 (Figure 7c). *Stage 1E magnetite–epidote–pyrite veins* have K-feldspar selvages and occur in the Goonumbla Volcanics in drill hole D245 at 810.96 m and in D247 at 461.72 m (Figure 7d).

Stage 2 – the Two-Thirty breccia complex

The Two-Thirty breccia is a subvertical dominantly polymict magmatic-hydrothermal breccia. Significant variation in cement *vs* clast abundance, clast-transport, attrition, and rotation occurs across the Two-Thirty breccia complex. As a result, the breccia is best described using facies and subfacies. The architecture of the breccia is described in the subsequent sections as well as supplementary material.

The Two-Thirty breccia complex is composed of three major breccia facies and several subfacies: divided into cemented (A and B facies; Supplementary Tables 3–5), igneous cemented (C facies, Supplementary Table 6) and tectonic-hydrothermal (F facies; Supplementary Table 7) breccias. The breccia post-dates Stage 1 potassic alteration and related veins that occur as or within clasts in the breccia. Cemented magmatic-hydrothermal breccias host high-grade mineralisation at Two-Thirty, there are four cemented breccia subfacies identified within the Two-Thirty breccia complex.

A1 breccia facies

The A1 facies has been subdivided into three subfacies: the A1-A breccia (Supplementary Table 3) is characterised by rare juvenile clasts (Figure 8a), including occurrences of truncated Stage 1C quartz–molybdenite–pyrite–chalcopyrite veins (Figure 8b). K-feldspar is the oldest Stage 2 infill mineral with large, euhedral crystals of K-feldspar the dominant breccia cement phase (Figure 8c). The overgrowth of other cement minerals is complex and in places contradictory. Euhedral to subhedral quartz + anhedral magnetite (quartz >> magnetite) are typically the second phase of cement. Quartz has locally cemented brecciated K-feldspar cement (Figure 8d), implying a second period of brecciation during the formation of A1 breccias.

Pyrite + chalcopyrite has overgrown quartz–magnetite in A1 breccias, and these comprise the second most abundant cement phase. Sulfide grains vary from euhedral to anhedral, and from a few mm to ~1 cm in diameter (Figure 8e). Carbonate ± minor fluorite has infilled the brecciated sulfide cement, after a third phase of brecciation (Figure 8f). There are some instances of fine ribbons of fluorite with no carbonate. The final cement stage has rare biotite + calcite, which

occurs as amorphous blebs and ribbons (Figure 8c). Calcite occurs as submillimetre clusters of anhedral crystals in a micro-crystalline biotite cement, which contains rare pyrite and chalcopyrite grains that are possibly clasts derived from earlier sulfide cement.

A2 breccia facies

The A2 facies is characterised by abundant quartz cement (Figure 9a, Supplementary Table 4). Early euhedral K-feldspar cement defines cockade textures around clasts; it is overgrown by euhedral to subhedral quartz with minor pyrite and K-Feldspar, and variable amounts of sand-sized matrix (Figure 9a). Quartz is overgrown by chalcopyrite–pyrite, with clasts of quartz occurring locally within the sulfide cement. The final stage of cementation is calcite–ankerite ± biotite–sphalerite and molybdenite, which occurs as anhedral masses amongst granular masses of euhedral quartz that appear to have been brecciated prior to carbonate precipitation. Minor fluorite bands occur where late carbonate cement is in direct contact with the early K-feldspar cement (Figure 9b). Late chlorite–sericite–pyrite veins crosscut the A2 breccia facies at 614 m in D247.

A3 breccias

The A3 facies and subfacies are matrix-rich with <10% cement (Supplementary Table 5). A3 breccias are interpreted to be located proximal to the centre of the breccia complex based on the poorly sorted, chaotic, polymict nature and degree of clast rounding, which suggests a more energetic brecciation process involving significant transport and abrasion. The cement paragenesis in the A3 breccia is similar to the A1 and A2 breccia facies. Euhedral K-feldspar cement occurs on clast margins. Subsequent brecciation is cemented by calcite ± fluorite. Chalcopyrite–pyrite and minor molybdenite occur as late, anhedral to subhedral masses up to a few mm in diameter. Disseminated molybdenite in the A3-breccia facies at 638 m in D240 has been dated using Re–Os.

Igneous-cemented breccias

Aplite-cemented breccias have similar clast, size, shapes, composition and abundances similar to the A1 breccia. These breccias are observed in a tens of centimetres intervals over 4 m from 836 m in D247 where it is gradational to the A1 breccia (Figure 9c; Supplementary Table 6).

Stage 2 – syn-brecciation alteration

Syn-brecciation alteration is varies spatially and in intensity within the Two-Thirty breccia complex. The alteration assemblages that affected each breccia facies are summarised in Table 5 and briefly described below. Stage 2 potassic alteration produced biotite–magnetite-alteration rinds around larger clasts in the A1-A, B, C and C1 breccia facies. Smaller clasts (< 3 cm) were pervasively biotite–magnetite altered. Secondary biotite is typically shreddy and has been partially replaced by later chlorite. *Stage 2 propylitic alteration* is most common in the A3 breccia facies where it is characterised by epidote ± pyrite that caused intense, pervasive and texturally destructive replacement of the matrix and smaller clasts. Propylitic alteration rinds on larger clasts have a thickness of < 2 cm.

Stage 2 – syn-breccia veins

Syn-brecciation veins define a halo to the Two-Thirty breccia complex and consist of multiple generations of quartz–pyrite veins that define a complex and locally contradictory paragenetic sequence. At least two generations of syn-breccia quartz–pyrite veins have been offset by *Stage 3A quartz–carbonate–pyrite–chalcopyrite–fluorite veins* that are associated with post-brecciation faulting but have a similar mineral assemblage to breccia cement.

Stage 2A – quartz–pyrite–biotite veins have a thicknesses < 3 mm with biotite–chlorite selvages and a K-feldspar alteration halos < 1 cm wide. Except for a single intercept of Goonumbla Volcanics that contained sheeted Stage 2A veins, no preferential orientation is shown. *Stage 2B – quartz–pyrite–muscovite–phengite veins* have limited abundance in the Two-Thirty breccia complex and are commonly < 1 mm thick with minor muscovite alteration halos a few millimetres wide.

Stage 3 – post-brecciation alteration and hydrothermal features

Post-brecciation features include numerous generations of calcite and quartz veins that are associated with selective carbonate alteration. *Stage 3A quartz–carbonate–pyrite–chalcopyrite–fluorite* veins vary from a few mm to several cm wide. Stage 3A veins have similar mineralogy to the A3 breccias. However crosscutting relationships indicate that they have a post brecciation timing. *Stage 3B – calcite–sphalerite–pyrite–chalcopyrite ± galena veins* are the second-most abundant vein type at Two-Thirty. Stage 3B veins, which vary from 1 mm to a few cm wide, are correlated with the Au-rich veins at the nearby E44 skarn (B. M. Jones, 1991; Stage 2 veins), and have significant potential to host high-grade epithermal mineralisation. *Stage 3C – epidote–pyrite veins* are typically <1 mm thick. Epidote is the most abundant mineral surrounding a central seam of subhedral pyrite. Stage 3C veins have propylitic alteration halos that are a few mm wide. Stage 3C veins offset Stage 2A quartz–pyrite–biotite veins. *Stage 3D – hematite veinlets* are typically <1 mm thick with chlorite ± epidote alteration halos <3 mm wide and no associated mineralisation. A Stage 3D hematite vein crosscuts a Stage 2A syn-brecciation quartz–K-feldspar vein at 823 m in D244. *Stage 3E – carbonate–anhydrite veins* contain a central seam of anhydrite and rare siderite selvedge, typically < 3 mm wide and crosscut all other vein generations. Stage 3E veins have no obvious alteration halos or associated mineralisation, except for a single occurrence of carbonate + bornite intersected at 418.2 m in D242. This is interpreted to relate to local remobilisation of copper from the mineralised breccia complex.

Fault and tectonic breccias

Small-scale faults are abundant at Two-Thirty, and fault breccias are particularly common in the Goonumbla Volcanics (Supplementary Table 7). Only minor occurrences of fault breccias were observed within the coherent facies of the Two-Thirty intrusive complex. Most of the fault breccia facies are monomict with occasional polymict examples; clasts with fault breccias typically reflect the local lithology. The F1-A facies are assigned a post-brecciation timing based on similar mineral assemblages to Stage 3B veins. The F1-A breccia facies are mostly phyllic-altered, moderate to well sorted, chaotic, monomict (occasionally polymict) quartz–pyrite–sphalerite–carbonate cemented fault breccias. Clasts in the F1-A facies are angular to subangular, and clast rotation is variable. Intense phyllic alteration halos of over 10 cm up to 1 m are generally associated with the F1-A breccia facies. The F1-B facies is correlated with Stage 3E carbonate veins implying a post-mineralisation timing. The F1-B facies are phyllic-altered moderate to poorly sorted, mononmict, carbonate–chlorite–phengite cemented fault breccias that are rarely associated with fault gouge and cataclasite. Clasts in the F1-B facies are typically elongate subangular to subrounded with a long axis aligned parallel to the fault plane. The F1-C facies is tentatively correlated with Stage 3A veins based on similarities in mineralogy and surrounding alteration. The F1-C facies has been crosscut by a Stage 3E vein at 319 m in D247 and has truncated the A1 breccia at 739 m in D247. The F1-C breccia facies, which are typically associated with texturally destructive phyllic alteration, are monomict poorly sorted quartz–pyrite–carbonate–fluorite–phengite cemented breccias that are typically limited to less than a few 10s of cm. A fault intersected at 739 m in D247 and 641 m in D240, which is inferred to have offset the Two-Thirty breccia body producing the F1-C breccia facies (Figure 4), is interpreted to have a dextral strike-slip motion based on slicken fibres observed in oriented core.

Mineralisation

Copper sulfide mineralisation at Two-Thirty is dominated by chalcopyrite. Copper assays generally increase downhole, and the highest grades are associated with the cemented magmatic-hydrothermal breccias. A small (<1 m) interval including visible bornite grains has been recognised in the Two-Thirty breccia complex. Further drilling is required to determine whether sulfide zonation is similar to Northparkes (i.e. whether a higher temperature bornite dominated sulfide zone, vein stockwork or cemented breccia is present at depth). Until the magmatic roots of the breccia complex are uncovered, these questions will remain unresolved.

High-grade mineralisation is associated with K-feldspar cemented and altered magmatic-hydrothermal breccias (breccia facies A and C; Figure 8). Gold mineralisation is hosted in skarn lenses and epithermal veins, and forms part of a distal halo to the magmatic-hydrothermal breccias that are characterised by elevated Ag, As, Sb, Sn and Zn. Telluride minerals have been documented in epithermal veins within the nearby E44 skarn prospect (B. M. Jones, 1991). Molybdenite occurs as disseminations in the Two-Thirty porphyry and in intervals of the A3 breccia facies (Figure 8b). The Two-Thirty prospect is the first significant occurrence of molybdenum mineralisation found near the Northparkes district. The vein-hosted molybdenite from E48 and E27 are rare examples of visible molybdenite in the Northparkes district.

Low–intermediate sulfidation mineralisation was first documented in the area near Two-Thirty by B. M. Jones (1991), who described three types of auriferous veins crosscutting skarn and associated with fault zones. These veins are broadly correlated with Stage 3B veins from this study. Jones (1991) describes cockade veins associated with quartz–sericite–pyrite alteration. Base-metal sulfides are the dominant sulfide species with local inclusions of altaite in galena and chalcopyrite in sphalerite. Intergrowths of hessite and altaite are common with lesser chalcopyrite and tennantite and minor petzite and bornite, free Au occurs as inclusions in all sulfide and telluride phases and is rarely observed as rims to pyrite grains (B. M. Jones, 1991).

Results

Geochronology

Zircon grain mounts were prepared from five representative intrusive rocks selected on the basis of their crosscutting relationships relative to mineralisation. The weighted average age of the most concordant group of zircons from each sample ranged from 450 to 439 Ma (Table 6). Most samples contained several zircons that have apparent ages younger than the main group and are ascribed to Pb-loss associated with high U–Th contents in zircons, as apparent in the concordia diagrams (Figure 10). Comparison of this data set with ages from other geochronological studies is presented in Figure 11.

An age of 450.5 ± 4.5 Ma (Figure 10; Table 6) was calculated from the analyses of 14 zircons from a mega clast of KHB-QMP within the Two-Thirty breccia. Seven additional analyses were rejected due to Ti and Fe inclusions, and Pb loss. A total of 13 of analyses were rejected due to Pb loss and elevated U. Thirty-six zircon analyses from the Two-Thirty porphyry returned an age of 448.0 ± 4.5 Ma (Figure 10a; Table 6). An age of 447.1 ± 4.5 Ma was calculated from 22 zircons obtained from the altered K-QMP sample (Figure 10b; Table 6). An additional five analyses were excluded due to Pb loss, and a further three analyses were rejected due to elevated U increasing the likelihood of Pb loss. A total of 31 zircons were analysed from the late-mineralisation monzonite porphyry, returning a mean age of 447.1 ± 4.5 Ma (Figure 10b). Effects of elevated U confounded three of the analyses, returning anomalously low ages (108, 109, 122 Ma). Forty-two zircons were analysed from a zero-porphyry sample. Sixteen of the analysed zircons were discarded during data reduction due to (1) high contents of common Pb, (2) Pb loss, and (3) inclusions or drill-through. Two discrete age populations were obtained from the remaining 29

analyses corresponding to ages of 455.5 Ma ± 4.4 and 438.8 ± 4.4 Ma (Table 6; Figures 10c and 11).

Re–Os dating of molybdenite from the A3 – breccia facies at 638 m in D240 indicates that the timing of this mineralisation (438.9 ± 1.4 Ma) is coeval with vein-hosted molybdenite at the E48 and E27 deposits within the Northparkes igneous complex (437.6 and 439.0 Ma; (Figure 11; Table 7). Notably, however, the Re content of the Two-Thirty molybdenite (225 ppm) is much lower than those from the Northparkes Intrusive Complex (1264–1717 ppm). These molybdenite ages are identical to that of the younger group of zircons obtained from the zero porphyry reported above (439 Ma), and significantly younger than the igneous crystallisation ages recorded by zircons from the other intrusions within the Two-Thirty intrusive complex. A comparison of the molybdenite and zircon ages indicates a difference of 9.1 ± 4.9 million years relative to the K-QMP, Two-Thirty and KHB-QMP porphyries (calculated in quadrature with decay constant uncertainty at 0.3% based on cross calibration of the two systems from Selby *et al.,* 2007).

The LA-ICPMS map of Re distribution in a single grain of molybdenite from the Two-Thirty breccia (Figure 12) shows concentric zoning from a high-Re core to a low-Re rim. In contrast, molybdenite from the Northparkes E48 deposit shows an oscillatory variation in Re content across the grain (possibly due to the fibrous habit of the molybdenite), whereas a grain from Northparkes E27 is relatively homogeneous in its Re distribution.

Discussion

The Two-Thirty breccia complex

The Two-Thirty breccia complex is composed of polyphase magmatic-hydrothermal breccias with the various breccia facies within the complex interpreted as the result of pulses of volatile exsolution from a hydrous magma. The numerous cement phases indicate at least five phases of brecciation and cementation. Magmatic cement, juvenile magmatic clasts and high-temperature mineral assemblages dominate the deepest intersections of the breccia. The magmatic-hydrothermal interpretation is based on the upward gradation from magmatic cement, to juvenile clasts and high-temperature cement minerals, with only minor matrix material. Morphology of the breccia indicates a pipe like structure but the vertical and lateral extent of the Two-Thirty breccia complex is only constrained by widely spaced and shallow drilling.

The Two-Thirty porphyry is interpreted to be the progenitor of the Two-Thirty breccia complex. Evidence for the genetic relationship is provided by the presence of juvenile clasts of Two-Thirty porphyry (including one occurrence of a probable unidirectional solidification texture fragment; Figure 8a, b) and the contact relationship between the intrusion and the A1 and igneous cemented breccia facies. High-temperature hydrothermal cement phases (K-feldspar, biotite, chalcopyrite, molybdenite; Figure 8b–d) and the local presence of igneous cement (Figure 9c) provide evidence for the magmatic-hydrothermal affinity of the Two-Thirty breccia complex (c.f., Sillitoe, 1985).

The dynamics of the Two-Thirty breccia complex can be inferred from the clast, compositions sizes, shapes, orientations and rotations. Large clasts with high degrees of clast rounding, and abundant matrix relative to cement are consistent with locally high energy brecciation. The A1 breccia facies is interpreted to have formed near the root zone of the breccia complex based on the proximity and gradational contact with the igneous (aplitic) cemented C1 breccia facies, the abundance of high-temperature cements, the variation from jigsaw fit to chaotic textures, and the presence of juvenile clasts. Preferential alignment of tabular clasts subparallel to the core axis (60°/113°) are interpreted to indicate that the clasts are derived from the spalling of wall rock, and that this drill hole is oriented subparallel to the walls of the breccia body.

The A2 breccia facies is characterised by common jigsaw fit textures, in contrast to the A1 breccia facies and is interpreted to indicate proximity to the edge of the breccia. In contrast, the A3 breccia facies is presumed to have formed at a location at, or near the centre of the breccia body where transport has caused significant attrition and mixing of clasts.

Timing of igneous intrusions and mineralisation at Two-Thirty

Ages obtained from LA-ICPMS U–Pb zircon analyses of the Two-Thirty intrusive complex indicate a timing of emplacement between 450.5 ± 5.5 Ma and 438.8 ± 4.4 Ma, spanning the range of phase 3 and phase 4 porphyries in the Macquarie Arc as defined by Glen, Crawford and Cooke (2007). Four of five units sampled from the Two-Thirty intrusive complex have Middle Ordovician ages (450.5 ± 4.5 Ma to 447.1 ± 4.5; Table 13), with the three mineralised intrusions dated here returning tightly constrained ages of 447–448 Ma. The pre-mineralisation KHB-QMP intrusion may be marginally older at 450.5 Ma although all four of these intrusions have ages that are identical within error (± 4.5 Ma).

Two sets of zircon ages (455.5 ± 4.4 and 438.8 ± 4.4 Ma) were obtained from a post-mineralisation zero porphyry at Two-Thirty. The 455.5 ± 4.4 Ma age is older than those obtained from the syn-mineralised intrusions and is interpreted as a zircon population that was inherited from the basal Goonumbla Volcanics and consistent with the age of 450.2 ± 4.8 Ma for the Goonumbla volcanics obtained by Butera *et al.* (2001) and within the constraints provided by fossil ages (460–450 Ma; Darriwilian to mid Eastonian; P. J. Jones, 1996). In contrast, the younger, Late Ordovician zircon age (438.8 ± 4.4 Ma) is interpreted to be the crystallisation age of this intrusion. Notably, the Re–Os age of the molybdenite from the A3 breccia facies (438.9 ± 2.2 Ma) is identical to the crystallisation age of this zero porphyry, perhaps suggesting a genetic link between zero porphyry emplacement and at least some deposition of molybdenite at this locality. The occurrence of the dated Two-Thirty molybdenite in the A3 breccia facies is consistent with a relatively late-stage of deposition and implies emplacement of multiple pulses of porphyries at Two-Thirty over a period of *ca* 10 Ma. However, discrimination of the timing of emplacement of individual intrusive phases is beyond the precision of the LA-ICPMS methods used in this study, and would require other techniques such as chemical abrasion isotope-dilution thermal ionisation mass spectrometry analysis (CA-ID-TIMS; Mattinson, 2005; Schaltegger *et al.*, 2015; Widmann *et al.*, 2019).

Porphyry deposits within the Macquarie Arc

Comparison of ages for the Two-Thirty and Northparkes intrusive complexes and other geochronological studies in the Macquarie Arc (Figure 11) further highlight the correlation of mineralisation ages for the Northparkes and Cadia districts (Harris *et al.*, 2014; Kemp *et al.,* 2020; Lickfold *et al.*, 2007; Wilson *et al.*, 2007) and the youngest igneous ages at Two-Thirty. The majority of high-grade, high-tonnage Cu–Au porphyry-related mineralisation in the Junee-Narromine and Molong belts of the Macquarie Arc are related to Group 4 (444–439 Ma) shoshonitic monzodiorite to quartz monzonite porphyries (Cooke *et al.*, 2007; Glen, Crawford, & Cooke, 2007; Heithersay & Walshe, 1995; Heithersay *et al.*, 1990; Holliday *et al.*, 2002; Lickfold *et al.*, 2003, 2007; Pacey *et al.*, 2019; Wells *et al.*, 2020; Wilson *et al.*, 2007). Two-Thirty is only the third documented occurrence of economically important porphyry-related mineralisation in the Macquarie Arc older than *ca* 444 Ma. The other examples are the calc-alkaline Marsden porphyry ~200 km to the south of Northparkes and the Copper Hill intrusive complex to the 80 km east of Northparkes (Perkins *et al.*, 1990, 1995).

Timing of magmatism and mineralisation at Two-Thirty compared to Northparkes

The age of mineralisation at Northparkes appears to be tightly constrained at 439 Ma based on ^{40}Ar–^{39}Ar dating of white mica alteration and U–Pb dating of zircons from intrusions in the

correlated Wombin Volcanics (Butera *et al.,* 2001; Perkins *et al.*, 1990). Bracketing ages of 444.2 ± 4.7 Ma and 436.7 ± 3.3 Ma based on U–Pb dating of zircon from pre- and post-mineralisation intrusives, respectively (Lickfold *et al.,* 2007), are consistent with this age assignment for the mineralisation at Northparkes. Our molybdenite ages from Northparkes (438–439 Ma; Table 7) are consistent with deposition of this phase during the main stage of mineralisation.

In contrast, the mineralised intrusions at Two-Thirty appear to be somewhat older, returning crystallisation ages of 447–448 Ma based on the zircon dating. Although the ages of zero porphyries at the two localities hint at an older episode of emplacement at Two-Thirty, the reported ages of these two post-mineralisation intrusives are identical within error (Northparkes 436.7 ± 3.3 Ma, Lickfold *et al.,* 2007; Two-Thirty 438.8 ± 4.4 Ma, this study). Also, in contrast to Northparkes, the dated molybdenite at Two-Thirty appears to post-date the main episode of mineralisation and is coeval with the zero porphyry at that locality. The close temporal correspondence between the main phase of Northparkes mineralisation and zero porphyry crystallisation, and molybdenite deposition at Two-Thirty is intriguing and may be indicative of a mineralising event that significantly post-dates the emplacement of the Two-Thirty porphyry and are more aligned with the timing of mineralisation at Northparkes. The disparity between zircon crystallisation ages and molybdenite deposition is inferred to be the product of a late hydrothermal overprint at Two-Thirty that corresponds within the timing of mineralisation at Northparkes. Further *in situ* investigation of Re distribution in molybdenite at Two-Thirty would increase the confidence in the ages obtained from multigrain dissolution of molybdenite.

Rhenium distributions in molybdenite from Two-Thirty and Northparkes

Although the ages of the molybdenites from Northparkes and Two-Thirty are identical, their contrasting Re contents (i.e., 1264–1717 ppm Northparkes *vs* 225 ppm for Two-Thirty; Table 7) suggests significant differences in magmatic-hydrothermal evolution or depositional conditions at the two sites. The high Re contents at Northparkes are similar to those of other alkalic-hosted porphyry deposits in the region such as Cadia (Kemp *et al.*, 2020; e.g., Wilson *et al.*, 2007) and Cu ± Au porphyry deposits generally (Barton *et al.*, 2020; Berzina *et al.*, 2005; Stein, 2014; Stein *et al.*, 2001; Terada *et al.*, 1971) . These high-Re molybdenites are strongly associated with intermediate-composition intrusions and have been ascribed to a significant mantle contribution to the magmas (Barton *et al.*, 2020; Berzina *et al.*, 2005; e.g., Stein *et al.*, 2001).

In contrast, lower Re concentrations in molybdenite are typically associated with more evolved magmatic-hydrothermal systems, although physicochemical conditions such as redox and the availability of reduced sulfur also exerts a strong control on molybdenite Re contents (Barton *et al.*, 2020). Therefore, the lower Re content of the Two-Thirty molybdenite relative to Ordovician porphyry mineralisation elsewhere in the Macquarie Arc may be indicating a difference in magmatic sources, which could be tested through additional radiogenic isotope studies (e.g., Rb–Sr, Sm–Nd, Lu–Hf). Alternatively, the fluids from which the molybdenite at Two-Thirty formed may be related to more evolved magmas or that they have a greater epithermal component. For example, highest grade gold at Two-Thirty is hosted in epithermal veins, and forms part of a distal halo to the magmatic-hydrothermal breccias that is characterised by elevated Ag, As, Sb, Sn and Zn. Telluride minerals have also been documented in epithermal veins within the nearby E44 prospect (B. M. Jones, 1991). This epithermal mineralisation appears to be a late overprint and may be represent the waning stages of a mineralising episode, but the source of Au–Te-rich low or intermediate sulfidation mineralisation at Two-Thirty requires further research.

The LA-ICPMS maps of single molybdenite grains from the three samples dated here show very different patterns of Re compositional variations, with two of them revealing strong spatial heterogeneities within the grains (Figure 12) that raise the possibility of alteration and/or

multi-stage growth of the molybdenites, which might compromise the Re–Os ages. For example, Aleinikoff *et al.* (2012) documented an occurrence of molybdenite overgrowths that yielded geologically meaningless Re–Os ages. However, that molybdenite had very low Re contents (<1 ppm) and the sample had a complex paragneiss with a multi-stage geological history that includes multiple generations of mineral dissolution and reprecipitation.

Heterogeneous Re distributions within molybdenite appear to be a common occurrence, with intra-grain concentrations ranging over several orders of magnitude in some cases (e.g., Barra *et al.*, 2017; Ciobanu *et al.*, 2013; Hogmalm *et al.*, 2019; Plotinskaya *et al.*, 2018; Rathkopf *et al.*, 2017), similar to that observed here for Northparkes and Two-Thirty. The causes of these small-scale compositional variations have not been clearly defined but must relate in some way to changes in fluid composition or conditions of deposition and/or grain growth. Unfortunately, the grain-scale studies have rarely been linked directly with detailed geochronology to demonstrate possible effects on Re–Os ages.

Although multiple stages of molybdenite deposition clearly has the potential to compromise Re–Os ages based on bulk concentrates (e.g., Aleinikoff *et al.,* 2012), a substantial time difference between the depositional events would be required, depending on the age of the deposit, the proportions of molybdenite deposited in each event, and the relative differences in Re content of the different generations. At Northparkes there is no substantial evidence for overprinting by later mineralisation, and the good agreement of the molybdenite ages with igneous events defined by zircon dating suggests that the molybdenite ages reported here likely reflect the timing of primary mineral deposition. Potential exists for overprinting to have occurred at Two-Thirty given the disparity between syn-mineralisation porphyry zircon crystallisation ages and molybdenite ages. However, possible confounding factors such as the extent to which the grains studied here are representative of their respective deposits, possible effects of crystallographic type and orientation of the molybdenite on the observed Re distributions, and possible overprints from alteration may need to be evaluated by future studies to better constrain the relationship of the molybdenite ages to the primary mineralisation.

Conclusions

The discovery of Two-Thirty is significant in that it is the first documented occurrence of a strongly mineralised magmatic-hydrothermal breccia in the Northparkes district, and the first significant evidence of low–intermediate sulfidation mineralisation associated with porphyry mineralisation in the Northparkes district. The discovery of high-grade Cu–Au–Mo mineralisation at the Two-Thirty prospect has broad implications for exploration in the Northparkes district and greater Macquarie Arc. The 448 ± 4.5 to 447.1 ± 4.5 Ma ages of emplacement of the syn-mineralisation porphyries within the Two-Thirty intrusive complex mostly pre-dates the emplacement of mineralising porphyries at Northparkes (*ca* 444 to 439 Ma; Lickfold *et al.*, 2007) and implies potential for two ore-forming periods within the Northparkes district which are broadly coincident with mineralisation timing at Cadia (Figure 11; Wilson *et al.*, 2007). The zircon age obtained from the post-mineralisation zero porphyry at Two-Thirty and a molybdenite age from the Two-Thirty breccia complex are coeval and within error of the syn-mineralisation intrusions at Northparkes, supporting the hypothesis of periodic release of melts and fluids from the underlying magma chambers in the Northparkes district (Lickfold *et al.*, 2007). Whether the economic mineralisation and generation of the Two-Thirty breccia is related to the emplacement of the Two-Thirty porphyry or some undiscovered intrusive phase remains unresolved and requires further drilling and research. The source and timing of high-grade Au low–intermediate sulfidation mineralisation remains undiscovered. Exploration at Two-Thirty is ongoing and may resolve some of the remaining questions in the near future.

Acknowledgements

The author would like to acknowledge the help and support of the analytical and professional staff at the University of Tasmania; Karin Orth, Sean Johnson, Anita Parhabakar-Fox, Aleksandr Stepanov, Matt Cracknell, Ayesha Ahmed, Jay Thompson, Brian McNulty, Margaret Hawke, Thomas Schaap and Thomas Osterson Northparkes Mines Exploration geologists Jeneata Owens, Corey Jago, Richard Lesh from Terrasearch, Katrina Thiel, Emily Cooke, Phillipa Cook; and finally Ms Danielle Pretty, Georgia Wells, Daemon and Christopher Black.

Funding

This research is funded by Australian Research Council sponsors of the Lachlan ARC Linkage Project 'LP160100483' CMOC-Northparkes, Rio Tinto, Evolution Mining, IMEx Consulting, Heron Resources, Sandfire Resources NL, New South Resources, AngloGold Ashanti, Alkane Resources, Geoscience Australia, The University of Tasmania, Australian National University, University of Melbourne, CCFS, Curtin University, the New South Wales, Tasmanian and Victorian state governments.

Data availability

The data that support the findings of this study are openly available in the University of Tasmania data repository at: DOI minted ASAP

References

Aleinikoff, J. N., Creaser, R. A., Lowers, H. A., Magee, C. W., & Grauch, R. I. (2012). Multiple age components in individual molybdenite grains. *Chemical Geology*, *300–301*, 55–60. https://doi.org/10.1016/j.chemgeo.2012.01.011

Armistead, S. E., Skirrow, R. G., Fraser, G. L., Huston, D. L., Champion, D. C., & Norman, M. D. (2017). *Gold and intrusion-related Mo–W mineral systems in the southern Thomson Orogen, New South Wales*. https://doi.org/10.11636/record.2017.005

Arundell, M. C. (1998). *The geology and mineralisation of the E31 copper–gold prospect, Goonumbla, N.S.W* (unpublished Masters of Economic Geology thesis). University of Tasmaina, Hobart, TAS, 82 p.

Barra, F., Deditius, A., Reich, M., Kilburn, M. R., Guagliardo, P., & Roberts, M. P. (2017). Dissecting the Re–Os molybdenite geochronometer. *Scientific Reports*, *7*(1), 16054. https://doi.org/10.1038/s41598-017-16380-8

Barton, I. F., Rathkopf, C. A., & Barton, M. D. (2020). Rhenium in molybdenite: a database approach to identifying geochemical controls on the distribution of a critical element. *Mining, Metallurgy and Exploration*, *37*(1), 21–37. https://doi.org/10.1007/s42461-019-00145-0

Berkley Geochronology Center. (2015*). Isoplot extension for Microsoft Excel 2007; a geochronological toolkit for Microsoft Excel: Vol. 3.75.* Berkley Geochronology Centre.

Berzina, A. N., Sotnikov, V. I., Economou-Eliopoulos, M., & Eliopoulos, D. G. (2005). Distribution of rhenium in molybdenite from porphyry Cu–Mo and Mo–Cu deposits of Russia (Siberia) and Mongolia. *Ore Geology Reviews*, *26*(1–2), 91–113. https://doi.org/10.1016/j.oregeorev.2004.12.002

Blackwell, J. L. (2010). *Characteristics and origins of breccias in a volcanic-hosted alkalic epithermal gold deposit, Ladolam, Lihir Island, Papua New Guinea* (unpublished PhD thesis). University of Tasmania, Hobart. TAS. p 190

Butera, K. M., Williams, I. S., Blevin, P. L., & Simpson, C. J. (2001). Zircon U–Pb dating of early Palaeozoic monzonitic intrusives from the Goonumbla area, New South Wales. *Australian Journal of Earth Sciences*, *48*(3), 457–464. https://doi.org/10.1046/j.1440-0952.2001.00870.x

Ciobanu, C. L., Cook, N. J., Kelson, C. R., Guerin, R., Kalleske, N., & Danyushevsky, L. (2013). Trace element heterogeneity in molybdenite fingerprints stages of mineralization. *Chemical Geology*, *347*, 175–189. https://doi.org/https://doi.org/10.1016/j.chemgeo.2013.03.011

Cooke, D. R., Wilson, A. J., House, M. J., Wolfe, R. C., Walshe, J. L., Lickfold, V., & Crawford, A. J. (2007). Alkalic porphyry Au–Cu and associated mineral deposits of the Ordovician to early Silurian Macquarie Arc, New South Wales. *Australian Journal of Earth Sciences*, *54*(2–3), 445–463. https://doi.org/10.1080/08120090601146771

Corbett, G. J., & Leach, T. M. (1998). Southwest Pacific Rim gold–copper systems; structure, alteration, and mineralization. In *Special Publication No. 6* (Vol. 6). Society of Economic Geologists.

Crawford, A. J. (2001). Tectono-magmatic development of the Ordovician volcanic belts in central western NSW, and the timing and location of porphyry-style mineralisation within the Macquarie Arc. In A. J. Crawford, D. R. Cooke, & R. A. Glen (Eds.), *NSW Ordovician SPIRT Report* (pp. 7.41–7.52). Centre for Ore Deposit Research.

Crawford, A. J., Glen, R. A., Cooke, D. R., & Percival, I. G. (2007). Geological evolution and metallogenesis of the Ordovician Macquarie Arc, Lachlan Orogen, New South Wales. *Australian Journal of Earth Sciences*, *54*(2–3), 137–141. https://doi.org/10.1080/08120090701221615

Crawford, A. J., Meffre, S., Squire, R. J., Barron, L. M., & Falloon, T. J. (2007). Middle and Late Ordovician magmatic evolution of the Macquarie Arc, Lachlan Orogen, New South Wales. *Australian Journal of Earth Sciences*, *54*(2–3), 181–214. https://doi.org/10.1080/08120090701227471

Danyushevsky, L., Robinson, P., Gilbert, S., Norman, M., Large, R., McGoldrick, P., & Shelley, M. (2011). Routine quantitative multi-element analysis of sulphide minerals by laser ablation ICP-MS: Standard development and consideration of matrix effects. *Geochemistry: Exploration, Environment, Analysis*, *11*(1), 51–60. https://doi.org/10.1144/1467-7873/09-244

Davies, A. G. S. (2002). *Geology and genesis of the Kelian gold deposit, East Kalimantan, Indonesia*. (unpublished PhD thesis) University of Tasmania, Hobart, TAS, 348 p.

Einaudi, M. T. (1997). Mapping altered and mineralized rocks; an introduction to the "Anaconda method." Stanford University.

Fox, N., Cooke, D. R., Harris, A. C., Collett, D., & Eastwood, G. (2015). Porphyry Au–Cu mineralization controlled by reactivation of an arc-transverse volcanosedimentary subbasin. *Geology*, *43*(9), 811–814. https://doi.org/10.1130/g36992.1

Glen, R. A., Crawford, A. J., & Cooke, D. R. (2007). Tectonic setting of porphyry Cu–Au mineralisation in the Ordovician–early Silurian Macquarie Arc, eastern Lachlan Orogen, New South Wales. *Australian Journal of Earth Sciences*, *54*(2–3), 465–479. https://doi.org/10.1080/08120090701221672

Glen, R. A., Crawford, A. J., Percival, I. G., & Barron, L. M. (2007). Early Ordovician development of the Macquarie Arc, Lachlan Orogen, New South Wales. *Australian Journal of Earth Sciences*, *54*(2–3), 167–179. https://doi.org/10.1080/08120090601146797

Glen, R. A., Percival, I. G., & Quinn, C. D. (2009). Ordovician continental margin terranes in the Lachlan Orogen, Australia: Implications for tectonics in an accretionary orogen along the east Gondwana margin. *Tectonics*, *28*(6), n/a–n/a. https://doi.org/10.1029/2009tc002446

Glen, R. A., Quinn, C. B., & Cooke, D. R. (2012). The Macquarie Arc, Lachlan Orogen, New South Wales; its evolution, tectonic setting and mineral deposits. *Episodes*, *35*(1), 177–186.

Glen, R. A., Spencer, R., Willmore, A., David, V., & Scott, R. J. (2007). Junee – Narromine Volcanic Belt, Macquarie Arc, Lachlan Orogen, New South Wales: components and structure. *Australian Journal of Earth Sciences*, *54*(2–3), 215–241. https://doi.org/10.1080/08120090601146805

Gregory, M. J., Lang, J. R., Gilbert, S., & Hoal, K. O. (2013). Geometallurgy of the Pebble porphyry copper–gold–molybdenum deposit, Alaska: Implications for gold distribution and paragenesis. *Economic Geology*, *108*(3), 463–482. https://doi.org/10.2113/econgeo.108.3.463

Harris, A. C., & Holcombe, R. J. (2014). Quartz vein emplacement mechanisms at the E26 porphyry Cu–Au deposit, New South Wales. *Economic Geology*, *109*(4), 1035–1050. https://doi.org/10.2113/econgeo.109.4.1035

Harris, A. C., Percival, I. G., Cooke, D. R., Tosdal, R. M., Fox, N., Allen, C. M., Tedder, I., McMillan, C., Dunham, P., & Collett, D. (2014). Marine volcanosedimentary basins hosting porphyry Au–Cu deposits, Cadia Valley, New South Wales, Australia. *Economic Geology*, *109*(4), 1117–1135. https://doi.org/10.2113/econgeo.109.4.1117

Harris, A. C., Cooke, D. R., Cuison, A. L. G., Groome, M., Wilson, A. J., Fox, N., Holliday, J., & Tosdal, R. (2020). Geologic evolution of Late Ordovician to early Silurian alkalic porphyry Au–Cu deposits at Cadia, New South Wales, Australia, In R. H. Sillitoe, R. J. Goldfarb, F. Robert & S. F. Simmons (Eds.), *Geology of the World's Major Gold Deposits and Provinces* (pp. 621–643). Society of Economic Geologists Special Publication No. 23. ISBN 978-1-629493-12-1 [Research Book Chapter]

Harrison, R. L., Maryono, A., Norris, M. S., Rohrlach, B. D., Cooke, D. R., Thompson, J. M., Creaser, R. A., & Thiede, D. S. (2018). Geochronology of the Tumpangpitu porphyry Au–Cu–Mo and high-sulfidation epithermal Au–Ag–Cu deposit: Evidence for pre- and postmineralization diatremes in the Tujuh Bukit district, southeast Java, Indonesia. *Economic Geology*, *113*(1), 163–192. https://doi.org/10.5382/econgeo.2018.4547

Heithersay, P. S., O'Neill, W. J., van der Helder, P., Moore, C. R., & Harbon, P. G. (1990). Goonumbla porphyry copper district; Endeavour 26 North, Endeavour 22 and Endeavour 27 copper–gold deposits. *Monograph Series – Australasian Institute of Mining and Metallurgy*, *14*, 1385–1398.

Heithersay, P. S., & Walshe, J. L. (1995). Endeavour 26 North; a porphyry copper–gold deposit in the Late Ordovician, shoshonitic Goonumbla volcanic complex, New South Wales, Australia. *Economic Geology*, *90*(6), 1506–1532. http://econgeol.geoscienceworld.org/content/90/6/1506.abstract

Hnatyshin, D., Creaser, R. A., Meffre, S., Stern, R. A., Wilkinson, J. J., & Turner, E. C. (2020). Understanding the microscale spatial distribution and mineralogical residency of Re in pyrite: Examples from carbonate-hosted Zn–Pb ores and implications for pyrite Re–Os geochronology. *Chemical Geology*, *533*, 119427. https://doi.org/10.1016/j.chemgeo.2019.119427

Hogmalm, K. J., Dahlgren, I., Fridolfsson, I., & Zack, T. (2019). First *in situ* Re–Os dating of molybdenite by LA-ICP-MS/MS. *Mineralium Deposita*, *54*(6), 821–828. https://doi.org/10.1007/s00126-019-00889-1

Holliday, J. R., Wilson, A. J., Blevin, P. L., Tedder, I. J., Dunham, P. D., & Pfitzner, M. (2002). Porphyry gold–copper mineralisation in the Cadia District, eastern Lachlan Fold Belt, New

South Wales, and its relationship to shoshonitic magmatism. *Mineralium Deposita*, *37*(1), 100–116. https://doi.org/10.1007/s00126-001-0233-8

Jones, B. M. (1991). *Geological setting and genesis fo the Endeavour 44 Au, Pb, Zn skarn, Parkes, NSW* (unpublished B.Sc Honours thesis) Australian National University, Canberra, ACT, 143 p.

Jones, G. J. (1985). The Goonumbla porphyry copper deposits, New South Wales. *Economic Geology*, *80*(3), 591–613. http://econgeol.geoscienceworld.org/content/80/3/591.abstract

Jones, P. J. (1996). AGSO Phanerozoic timescale 1995: wall chart and explanatory notes. In P. J. Jones (compiler) with personnel of the AGSO Timescale Calibration and Development Project 1995 (O. Australian Geological Survey (ed.); Issue accessed from http://nla.gov.au/nla.cat–vn961366). Oxford University Press.

Kemp, A. I. S., Blevin, P. L., & Norman, M. D. (2020). A SIMS U–Pb (zircon) and Re–Os (molybdenite) isotope study of the early Paleozoic Macquarie Arc, southeastern Australia: Implications for the tectono-magmatic evolution of the paleo-Pacific Gondwana margin. *Gondwana Research*. https://doi.org/10.1016/j.gr.2019.12.015

Krynen, J. P., Sherwin, L., & Clarke, I. (1990). Stratigraphy and structure. *Records of the Geological Survey of New South Wales*, *23*(1), 1–76.

Large, R. R., Danyushevsky, L., Hollit, C., Maslennikov, V., Meffre, S., Gilbert, S., Bull, S., Scott, R., Emsbo, P., Thomas, H., Singh, B., & Foster, J. (2009). Gold and trace element zonation in pyrite using a laser imaging technique: Implications for the timing of gold in orogenic and Carlin-style sediment-hosted deposits. *Economic Geology*, *104*(5), 635–668. https://doi.org/10.2113/gsecongeo.104.5.635

Lickfold, V. (2002). *Intrusive history and volatile evolution of the Endeavour porphyry Cu–Au deposits, Goonumbla district, NSW, Australia* (unpublished PhD Thesis). University of Tasmania, Hobart, TAS, 232 p.

Lickfold, V., Cooke, D. R., Crawford, A. J., & Fanning, C. M. (2007). Shoshonitic magmatism and the formation of the Northparkes porphyry Cu–Au deposits, New South Wales. *Australian Journal of Earth Sciences*, *54*(2–3), 417–444. https://doi.org/10.1080/08120090601175754

Lickfold, V., Cooke, D. R., Smith, S. G., & Ullrich, T. D. (2003). Endeavour copper–gold porphyry deposits, Northparkes, New South Wales: Intrusive history and fluid evolution. *Economic Geology*, *98*(8), 1607–1636. https://doi.org/10.2113/gsecongeo.98.8.1607

Mattinson, J. M. (2005). Zircon U/Pb chemical abrasion (CA-TIMS) method; combined annealing and multi-step partial dissolution analysis for improved precision and accuracy of zircon ages. *Chemical Geology*, *220*(1–2), 47–66. https://doi.org/10.1016/j.chemgeo.2005.03.011

McPhie, J., Doyle, M., & Allen, R. (1993). *Volcanic textures; a guide to the interpretation of textures in volcanic rocks:* (196 p.). University of Tasmania, Centre for Ore Deposit and Exploration Studies.

Meffre, S., Belousova, E., Zhukova, I., Leslie, C., Wells, T. J., & Cuison, L. (2018). The Cambrian Island Arc basement of the Macquarie Arc, SE Australia. *Abstracts Australian Geoscience Council Convention,* Adelaide, SA.

Mort, K., & Woodcock, N. H. (2008). Quantifying fault breccia geometry; Dent Fault, NW England. *Journal of Structural Geology*, *30*(6), 701–709. https://doi.org/10.1016/j.jsg.2008.02.005

Norman, M., Bennett, V., & McCulloch, M. (2004). New Re–Os ages of molybdenite from granite-related deposits of Eastern Australia using an improved multi-collector ICP-MS technique. *MORE-SGEG Symposium, July 2004*.

Pacey, A., Wilkinson, J. J., Owens, J., Priest, D., Cooke, D. R., Miller, I. L., & Millar, I. L. (2019). The anatomy of an alkalic porphyry Cu–Au system: geology and alteration at Northparkes mines, New South Wales, Australia. *Economic Geology*, *114*(3), 441–472. https://doi.org/10.5382/econgeo.4644

Percival, I. G., & Glen, R. A. (2007). Ordovician to earliest Silurian history of the Macquarie Arc, Lachlan Orogen, New South Wales. *Australian Journal of Earth Sciences*, *54*(2–3), 143–165. https://doi.org/10.1080/08120090601146789

Perkins, C., McDougall, I., Claoue-Long, J., & Heithersay, P. S. (1990). $^{40}Ar/^{39}Ar$ and U–Pb geochronology of the Goonumbla porphyry Cu–Au deposits, New South Wales, Australia. *Economic Geology*, *85*(8), 1808–1824. http://econgeol.geoscienceworld.org/content/85/8/1808.abstract

Perkins, C., Walshe, J. L., & Morrison, G. (1995). Metallogenic episodes of the Tasman Fold Belt system, eastern Australia. *Economic Geology*, *90*(6), 1443–1466. https://doi.org/10.2113/gsecongeo.90.6.1443

Plotinskaya, O. Y., Abramova, V. D., Groznova, E. O., Tessalina, S. G., Seltmann, R., & Spratt, J. (2018). Trace-element geochemistry of molybdenite from porphyry Cu deposits of the Birgilda-Tomino ore cluster (South Urals, Russia). *Mineralogical Magazine*, *82*(S1), S281–S306. https://doi.org/10.1180/minmag.2017.081.106

Rathkopf, C., Mazdab, F., Barton, I., & Barton, M. D. (2017). Grain scale and deposit scale heterogeneity of Re distribution in molybdenite at the Bagdad porphyry Cu–Mo deposit, Arizona. *Journal of Geochemical Exploration*, *178*, 45–54. https://doi.org/10.1016/j.gexplo.2017.03.011

Rinne, M. L., Cooke, D. R., Harris, A. C., Finn, D. J., Allen, C. M., Heizler, M. T., & Creaser, R. A. (2018). Geology and geochronology of the Golpu porphyry and Wafi epithermal deposit, Morobe Province, Papua New Guinea. *Economic Geology*, *113*(1), 271–294. https://doi.org/10.5382/econgeo.2018.4551

Robertson, P. K., & Callaghan, J. F. O. (1988). Display of Remotely Sensed Imagery. *IEEE Transactions on Geoscience and Remote Sensing*, *26*(1), 49–59.

Rush, J. A. (2013). *Geology of the Marsden Cu–Au Porphyry, NSW* (unpublished *B.Sc Hon*ours thesis). University of Tasmania, Hobart, TAS, 96 p.

Schaltegger, U., Schmitt, A. K., & Horstwood, M. S. A. (2015). U–Th–Pb zircon geochronology by ID-TIMS, SIMS, and laser ablation ICP-MS: Recipes, interpretations, and opportunities. *Chemical Geology*, *402*, 89–110. https://doi.org/10.1016/j.chemgeo.2015.02.028

Seedorff, E., Dilles, J. H., Proffett Jr., J. M., Einaudi, M. T., Zurcher, L., Stavast, W. J. A., Johnson, D. A., & Barton, M. D. (2005). Porphyry deposits; characteristics and origin of hypogene features. *Economic Geology; One Hundredth Anniversary Volume, 1905–2005*, 251–298.

Selby, D., Creaser, R. A., Stein, H. J., Markey, R. J., & Hannah, J. L. (2007). Assessment of the 187Re decay constant by cross calibration of Re-Os molybdenite and U-Pb zircon chronometers in magmatic ore systems. *Geochimica et Cosmochimica Acta*, *71*(8), 1999–2013. https://doi.org/10.1016/j.gca.2007.01.008

Shirey, S. B., & Walker, R. J. (1995). Carius tube digestion for low-blank rhenium–osmium analysis. *Analytical Chemistry*, *34*, 2136–2141. https://doi.org/10.1021/ac00109a036

Sillitoe, R. H. (1985). Ore-related breccias in volcanoplutonic arcs. *Economic Geology*, *80*(6), 1467–1514. https://doi.org/10.2113/gsecongeo.80.6.1467

Simpson, C. J., Cas, R. A. F., & Arundell, M. C. (2005). Volcanic evolution of a long-lived Ordovician island-arc province in the Parkes region of the Lachlan fold belt, southeastern Australia. *Australian Journal of Earth Sciences*, *52*(6), 863–886. https://doi.org/10.1080/08120090500304273

Smith, N., & van der Walt, S. (2015). A better defualt colourmap for Matplotlib. *SciPy 2015 – Scientific Computing with Python*.

Smith, S., Mowat, B., & Sharry, M. (2004). Macquarie Arc porphyry Au–Cu systems; a review of the critical exploration features. *Abstracts – Geological Society of Australia*, *74*, 51–62.

Stacey, J. S., & Kramers, J. D. (1975). Approximation of terrestrial lead isotope evolution by a two-stage model. *Earth and Planetary Science Letters*, *26*(2), 207–221. https://doi.org/10.1016/0012-821X(75)90088-6

Steadman, J. A., Large, R. R., Meffre, S., Olin, P. H., Danyushevsky, L. V, Gregory, D. D., Belousov, I., Lounejeva, E., Ireland, T. R., & Holden, P. (2015). Synsedimentary to early diagenetic gold in black shale-hosted pyrite nodules at the Golden Mile Deposit, Kalgoorlie, Western Australia. *Economic Geology*, *110*(5), 1157–1191. https://doi.org/10.2113/econgeo.110.5.1157

Stein, H. J. (2014). Dating and tracing the history of ore formation. In *Treatise on Geochemistry: Second Edition* (2nd ed., Vol. 13). Elsevier Ltd. https://doi.org/10.1016/B978-0-08-095975-7.01104-9

Stein, H. J., Markey, R. J., Morgan, J. W., Hannah, J. L., & Scherstén, A. (2001). The remarkable Re–Os chronometer in molybdenite: How and why it works. *Terra Nova*, *13*(6), 479–486. https://doi.org/10.1046/j.1365-3121.2001.00395.x

Streckeisen, A. (1976). To each plutonic rock its proper name. *Earth-Science Reviews*, *12*(1), 1–33. https://doi.org/10.1016/0012-8252(76)90052-0

Sykora, S., Cooke, D. R., Meffre, S., Stephanov, A. S., Gardner, K., Scott, R., Selley, D., & Harris, A. C. (2018). Evolution of pyrite trace element compositions from porphyry-style and epithermal conditions at the Lihir gold deposit: Implications for ore genesis and mineral processing. *Economic Geology*, *113*(1), 193–208. https://doi.org/10.5382/econgeo.2018.4548

Sykora, S., Selley, D., Cooke, D. R., & Harris, A. C. (2018). The structure and significance of anhydrite-bearing vein arrays, Lienetz orebody, Lihir Gold Deposit, Papua New Guinea. *Economic Geology*, *113*(1), 237–270. https://doi.org/10.5382/econgeo.2018.4550

Tera, F., & Wasserburg, G. J. (1972). U–Th–Pb systematics in three Apollo 14 basalts and the problem of initial Pb in lunar rocks. *Earth and Planetary Science Letters*, *14*(3), 281–304. https://doi.org/http://dx.doi.org/10.1016/0012-821X(72)90128-8

Terada, K., Osaki, S., Ishihara, S. & Kiba, T. (1971). Distribution of rhenium in molybdenites from Japan. *Geochemical Journal*, *4*, 123–141. https://doi.org/10.2343/geochemj.4.123

Thompson, T. B. (1993). Hydrothermal breccias. *Special Publication – Geological Society of Nevada*, *19*, 4.

Wells, T. J., Meffre, S., Cooke, D. R., Steadman, J. A., & Hoye, J. L. (2020). Porphyry fertility in the Northparkes district: indicators from whole-rock geochemistry. *Australian Journal of Earth Sciences*, *5*(67), 717–738. https://doi.org/10.1080/08120099.2020.1715477

Widmann, P., Davies, J. H. F. L., & Schaltegger, U. (2019). Calibrating chemical abrasion: Its effects on zircon crystal structure, chemical composition and U–Pb age. *Chemical Geology*, *511*, 1–10. https://doi.org/10.1016/j.chemgeo.2019.02.026

Wilson, A. J., Cooke, D. R., & Harper, B. L. (2003). The Ridgeway gold–copper deposit; a high-grade alkalic porphyry deposit in the Lachlan Fold Belt, New South Wales, Australia. *Economic Geology*, *98*(8), 1637–1666. https://doi.org/10.2113/gsecongeo.98.8.1637

Wilson, A. J., Cooke, D. R., Stein, H. J., Fanning, C. M., Holliday, J. R., & Tedder, I. J. (2007). U–Pb and Re–Os geochronologic evidence for two alkalic porphyry ore-forming events in the Cadia District, New South Wales, Australia. *Economic Geology*, *102*(1), 3–26. https://doi.org/10.2113/gsecongeo.102.1.3

Zhang, Q., Buckman, S., Bennett, V. C., & Nutman, A. (2019). Inception and early evolution of the Ordovician Macquarie Arc of Eastern Gondwana margin: Zircon U–Pb–Hf evidence from the Molong Volcanic Belt, Lachlan Orogen. *Lithos*, *326–327*(January), 513–528. https://doi.org/10.1016/j.lithos.2019.01.008

Zukowski, W. (2010). *Geology and mineralisation of the Endeavour 41 Gold Deposit, Cowal District, NSW, Australia* (unpublished PhD thesis). CODES, University of Tasmania.

Zukowski, W., Cooke, D. R., Deyell, C. L., McInnes, P., & Simpson, K. (2014). Genesis and exploration implications of epithermal gold mineralization and porphyry-style alteration at the Endeavour 41 prospect, Cowal District, New South Wales, Australia. *Economic Geology*, *109*(4), 1079–1115. https://doi.org/10.2113/econgeo.109.4.1079

Figure and table captions

Figure 1. Eastern Australia and the location of the three major volcanic belts of the Macquarie Arc.

Figure 2. Geology of the Two-Thirty and surrounding prospects (modified after B. M. Jones, 1991) its location relative to the Northparkes porphyry deposits. District map modified after Arundell (1998) and Simpson *et al.* (2005) after maps by Heithersay *et al.* (1990) and Pacey (2019).

Figure 3. Paragenesis of the Two-Thirty prospect.

Figure 4. Schematic cross-section of 5 holes from the drill campaign that intersected high-grade mineralisation at the Two-Thirty.

Figure 5. Outcrop photos of (a) Mafic enclave in KHB-QMP and (b) KHB-QMP xenoltih in Two-Thirty porphyry intrusion.

Figure 6. (a) BQM; (b) K-QMP; (c) chalcopyrite bleb in K-QMP; (d) Two-Thirty porphyry; (e) blocky K-feldspar fracture fill with similar infill phases as the A1 breccia facies in Two-Thirty porphyry near contact with the A1 breccia; and (f) hematite-dusted zero porphyry.

Figure 7. (a) Biotite–magnetite alteration in Two-Thirty breccia; (b) sheeted quartz veins in KHB-QMP; (c) altered KHB-QMP with sheeted veins and late carbonate crosscutting; and (d) magnetite–epidote–pyrite veins with K-feldspar selvages occur in the Goonumbla Volcanics in drill hole D245 at 810.96 m and in D247 at 461.72 m. These rare occurrences are not observed within the Two-Thirty breccia itself.

Figure 8. (a) Juvenile clast of the two-thirty porphyry in the A1 breccia facies; (b) truncated quartz–molybdenite vein; (c) K-feldspar cement with hematite dusting in the A1 breccia; (d) brecciated early K-feldspar cement in a quartz vein; (e) open space fill by late chalcopyrite + pyrite; and (f) carbonate + fluorite cement phase in the A1 breccia.

Figure 9. Two-Thirty breccia complex A2 and A3 facies: (a) quartz dominant cement with fractured earlier K-feldspar as cockade textures on clasts; (b) fluorite bands with carbonate and brecciated K-feldspar infill; and (c) igneous cement in the C1 breccia facies toward the base on the Two-Thirty breccia. This breccia facies is gradational to the A1 facies.

Figure 10. Zircon U–Pb concordia diagrams for selected phases from the Two-Thirty intrusive complex; 2 σ error is represented by ellipse. Ellipse colour represents U content in zircons as an indicator of metamictisation: (a) NP16TW168 the Two-Thirty porphyry; (b) NP16TW133 altered K-QMP; (c) older of the two populations from the NP16TW122 zero porphyry sample; (d) younger of the two populations from the zero porphyry; (e) NP16TW053 monzonite sample; and (f) NP16TW077 KHB-QMP pre-mineralisation porphyry.

Figure 11. Two-Thirty intrusive complex in the context of regional geochronology, modified after Rush (2013) and Zukowski (2010). Abbreviation denote the following qtz, quartz; ccpy, chalcopyrite; cal, calcite; mlb, molybdenite.

Figure 12. Distribution of Mo and Re in molybdenite grains from across the Northparkes district: (a, d) NP17TW55 vein-hosted molybdenite from E48; (b, e) vein-hosted molybdenite from E27; (c, f) molybdenite as a late infill mineral in the A3 magmatic-hydrothermal breccia facies at Two-Thirty. Re distribution in molybdenite from E48 and Two-Thirty varies by an order of magnitude. At E27

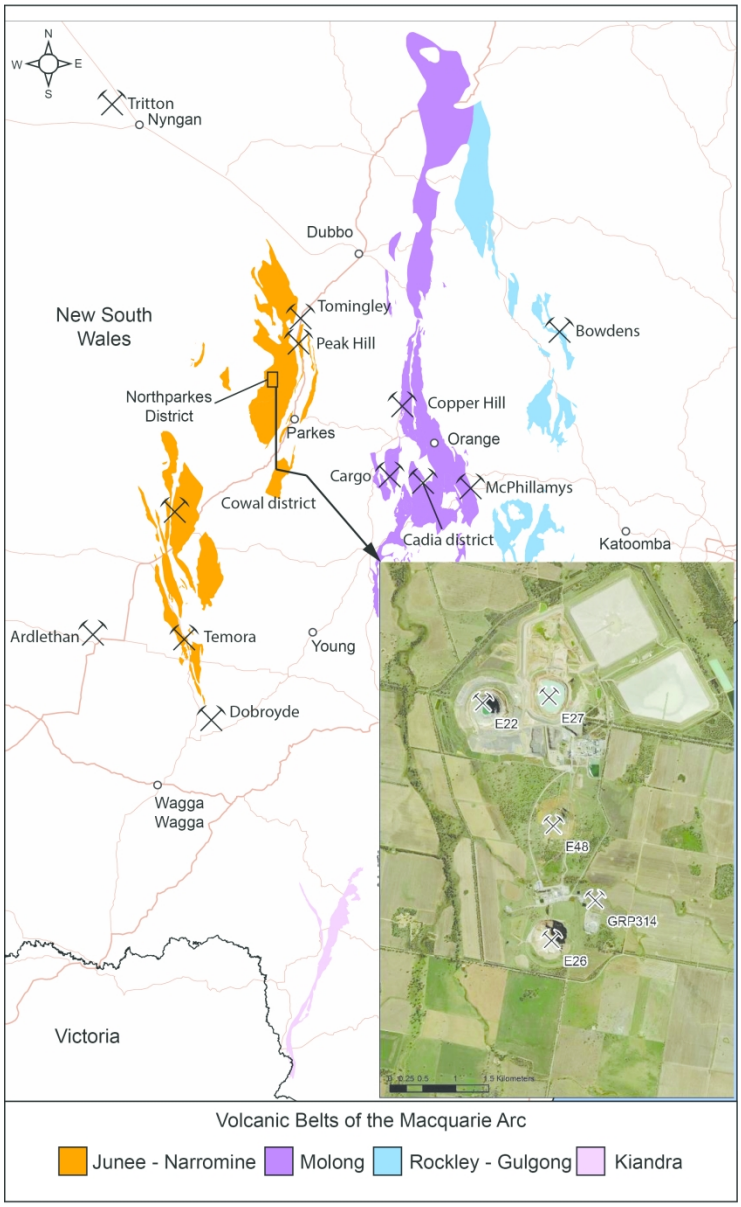

Figure 1: Eastern Australia and the location of the three major volcanic belts of the Macquarie Arc.

185x302mm (300 x 300 DPI)

Table 1: Significant intercepts from exploration drilling at Two-Thirty

Drill hole	Interval (m)	From (m)	Au (g/t)	Cu (%)	Mo (ppm)
0.1% Cu cutoff 20 m minimum intercept and 20 m internal dilution					
D240	272	500	0.09	0.10	166
D245	94	772	0.07	0.14	49
D251	154	548	0.06	0.14	34
	94	758	0.3	0.49	200
	132	658	0.06	0.1	47
	212.2	851.8	0.03	0.19	99
D252	146	764	0.07	0.1	50
	176	190	0.6	0.11	10
0.5% cutoff, 10 m minimum intercept and 20 m internal dilution					
D240	42	16	0.64		
D244	10	336	0.52		
D248W1	34	806	0.61		
	90	452	0.54		
D249	20	42	0.54		
	17	39	1.58		
	20	274	0.67		
D240	1	46	10.4		
D255	5		5.3		
	2		18		
D256	1		25		
	19		15		

Table 2: Magmatic evolution of the Macquarie Arc, (Crawford et al., 2007; Percival and Glen, 2007; Zukowski, 2010; Rush, 2013)

Phase	Magmatic suite	Tectonic setting	Description	Age (Ma)
1	High-K calc-alkaline to shoshonitic	Pre-accretionary	Supra-subductional above a west-dipping subduction zone	495- 475
Hiatus	-	-	Related to the extension of the Wagga back arc basin	475- 466
2	Medium to high-K calc-alkaline later stages tend toward shoshonitic	Pre-accretionary	Supra-subductional	466- 456
Hiatus	-	-	Not arc wide but in localised characterised by carbonate accumulation	450- 455
3	Shoshonitic intrusions and wide spread, small volume high-K calc alkaline	Pre-accretionary	Reversal of polarity of subduction from west-dipping to east-dipping in response to lock up of slab roll back or seamount collision (Meffre et al., 2007)	456- 443
4	Shoshonitic	Syn-accretionary	Supra-subductional initial facies were extrusive (456-443 Ma); Post collisional relaxation (444-437 Ma) is associated with highly mineralised alkalic porphyries at Cadia and Northparkes	444- 437

Table 3: Summary of the Goonumbla Volcanic Complex

Formation	Composition	Description of coherent phases	Thickness	Age (Ma)	References
Nelungaloo Volcanics	Coherent andesite overlain by conglomerates sandstones	Plagioclase + clinopyroxene + olivine + Fe-Ti oxide phyric andesites	~650 m	482 – 471	Krynen et al. (1990), Crawford et al. (2007), Lickfold et al. (2007)
Goonumbla Volcanics	Basaltic andesite – trachyandesite lavas with subordinate volcanics	Apatite- free, olivine bearing, basaltic and basaltic andesite lava; plagioclase + augite + Fe-Ti oxides + apatite phenocrysts in a variably glassy matrix	2.5 – 4 km	460 - 444	Butera et al. (2001); Lickfold et al. (2007)
Wombin Volcanics	Ignimbrites, polymict volcaniclastic breccias and volcanic sandstones, with porphyritic trachyandesites and trachytic lavas	Pyroxene poor trachyandesite, biotite trachyandesite, crystal crowded trachyandesite, microcrystalline hematite imparts a dark red colour	700-1000 m	444 – 434	Perkins et al. (1990); Butera et al. (2001); Simpson et al. (2005); Lickfold et al. (2007)

Table 4: Two-Thirty Intrusive complex

Intrusive phase	Composition	Grainsize	Description	Mineralisation
Pre – early mineral intrusions				
Mafic dykes	Basaltic composition	<1 mm	Present as enclaves in KBH-QMP	None
K-feldspar-hornblende-biotite phyric QMP	70-80% plagioclase, 20-30% K-feldspar ± 5% hornblende phenocrysts with minor ~2-3% biotite + magnetite ± leucoxene; fine grained to granular groundmass with rare euhedral quartz	~2 mm	Equigranular to porphyritic; Variably megacrystic; K-feldspar phenocrysts commonly with poikilitic inclusions	Disseminated chalcopyrite and pyrite ± porphyry-style quartz stockwork veining
Biotite-quartz monzonite	Euhedral biotite, plagioclase, alkali feldspar, and quartz	~2 mm	Equigranular to weakly porphyritic	Disseminated pyrite ± chalcopyrite
Syn – mineral intrusions				
Two-Thirty Porphyry	70% K-feldspar 30% plagioclase, phenocrysts ± 5% clinopyroxene + biotite + magnetite + hornblende ± leucoxene after titanomagnetite; very fine grained to aphanitic feldspar + quartz groundmass		Sparse to crystal crowded porphyritic textures Subhedral K-feldspar rims euhedral plagioclase and form (<5 mm) clusters	Disseminated pyrite-chalcopyrite-molybdenite; minor pyrite veinlets
K-feldspar phyric QMP	30-40% plagioclase and alkali feldspar phenocrysts with minor (<2%) magnetite + biotite ± hornblende in an aphanitic to very fine-grained alkali-feldspar + quartz groundmass.	Weakly to strongly porphyritic	Variable from pale pink to dark red; sparsely K-feldspar phyric	Disseminated pyrite and chalcopyrite, rare blebs of pyrite, chalcopyrite Quartz veins ± a central seam of K-feldspar
Late – post mineral intrusions				
Monzonite porphyry	Plagioclase and K-feldspar phyric with minor magnetite in a granular plagioclase + K-feldspar groundmass		Sparsely to moderately porphyritic with no K-feldspar megacrysts	Typified by a distinct lack of chalcopyrite, pyrite or anhydrite blebs
Zero porphyry	Plagioclase, alkali-feldspar, augite + biotite + magnetite + anhydrite phenocrysts in aphanitic to fine-grained groundmass of alkali-feldspar 95%		Variable from aphanitic to crystal crowded typically with a gradational contact	None
Mafic dykes	Basaltic composition	<1 mm	< 1 m wide with a consistent NE strike and a subvertical dip	

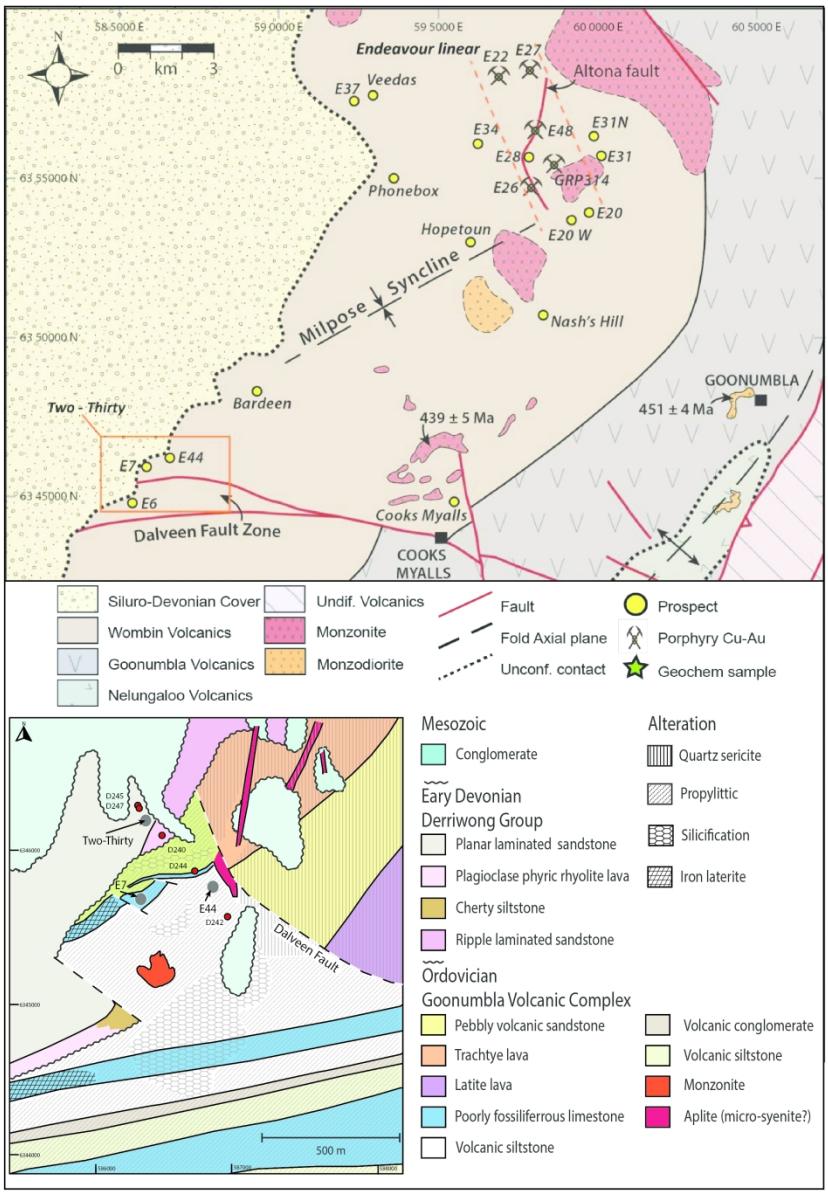

Figure 2: Geology of the Two-Thirty and surrounding prospects, (Modified after Jones (1991) and its location relative to the Northparkes porphyry deposits. District map modified after Arundell, (1998) and Simpson et al., (2005) after maps by Heithersay et al. (1990) and Pacey (2016).

210x297mm (300 x 300 DPI)

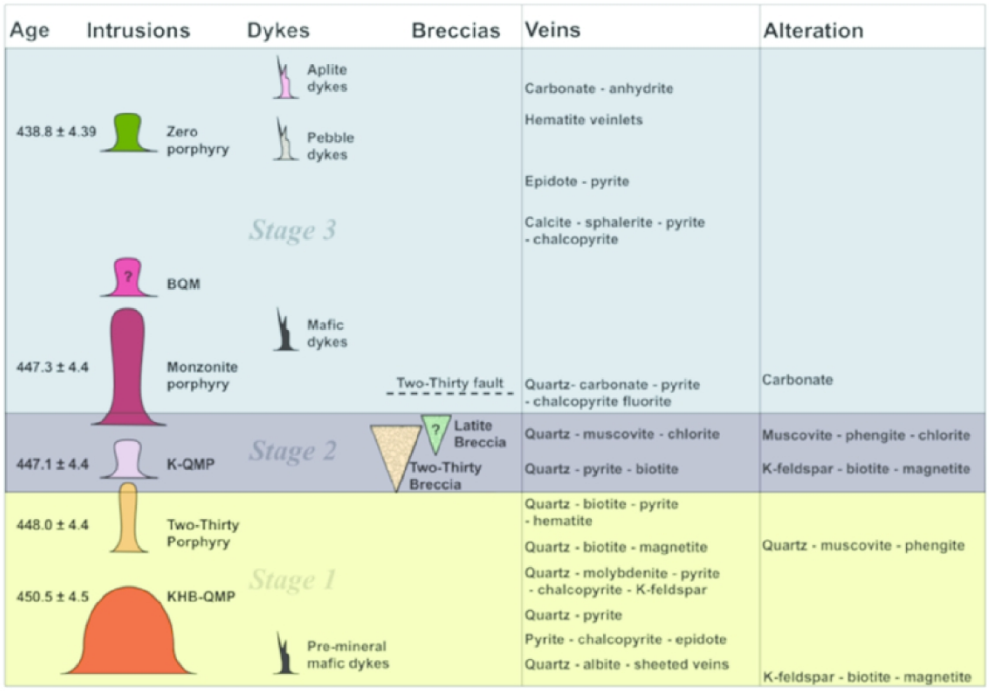

Figure 3: Paragenesis of the Two-Thirty prospect.

210x148mm (300 x 300 DPI)

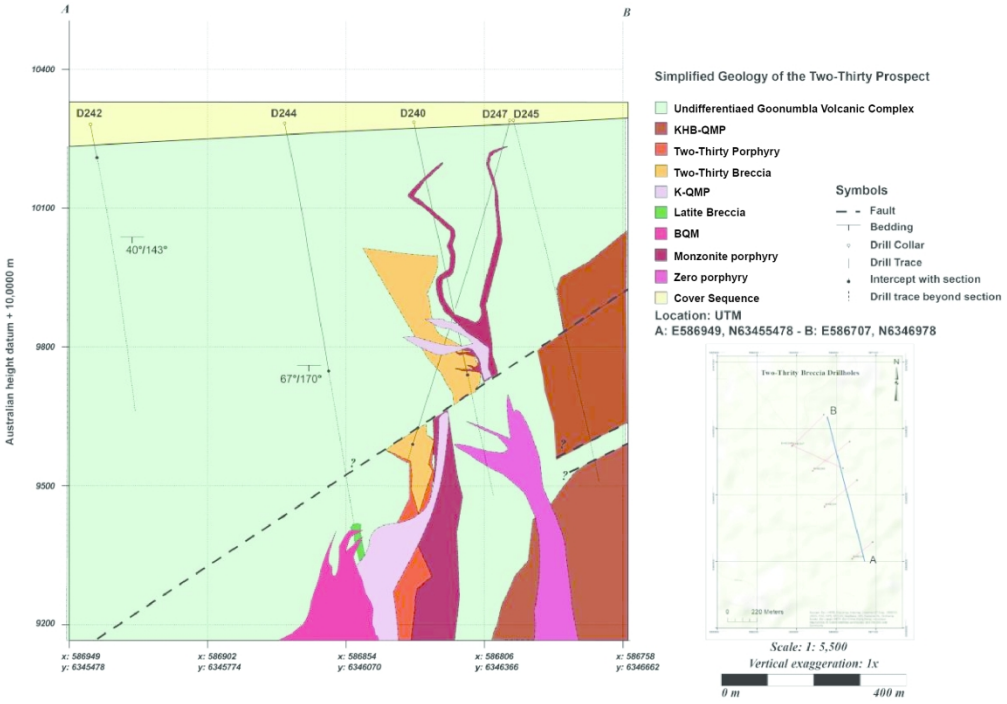

Figure 4: Schematic cross-section of 5 holes from the drill campaign that intersected high grade mineralisation at the Two-Thirty.

210x146mm (300 x 300 DPI)

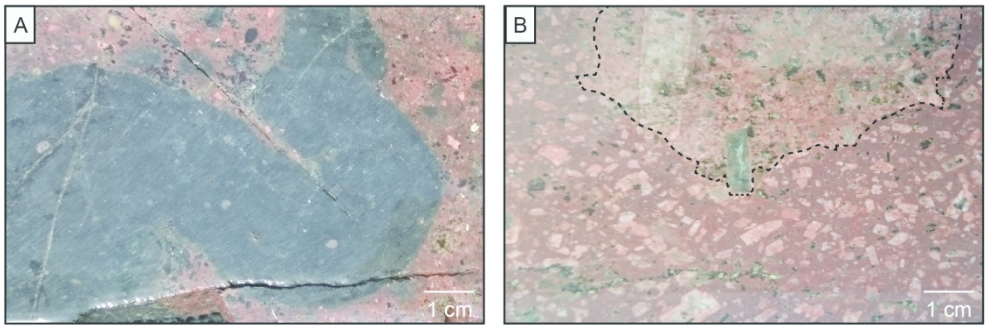

Figure 5: (a) mafic enclave in KHB-QMP (b) KHB-QMP xenoltih in Two-Thirty porphyry intrusion.

186x64mm (300 x 300 DPI)

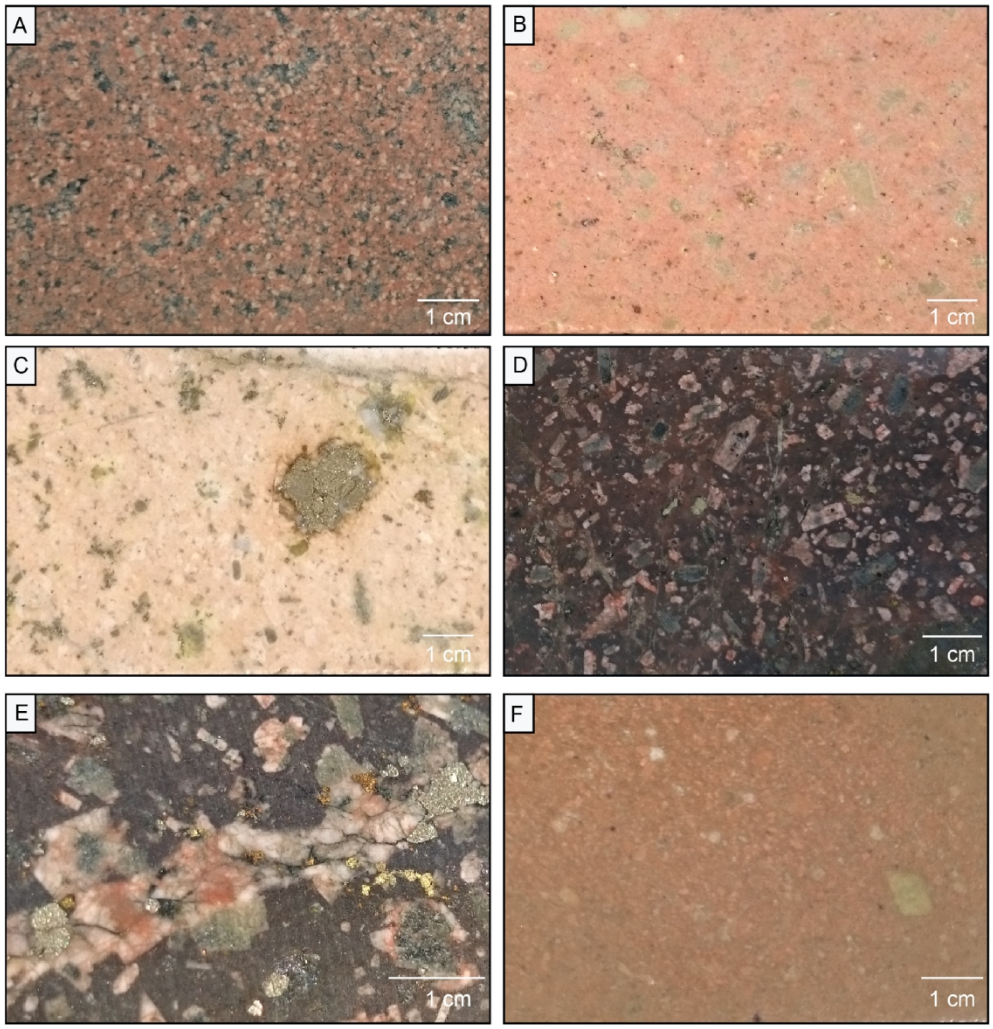

Figure 6: (a) BQM (b) K-QMP (c) Chalcopyrite bleb in K-QMP (d) Two-Thirty porphyry (e) Blocky K-feldspar fracture fill with similar infill phases as the A1 breccia facies in Two-Thirty porphyry near contact with the A1 breccia (f) Hematite dusted zero porphyry.

210x215mm (300 x 300 DPI)

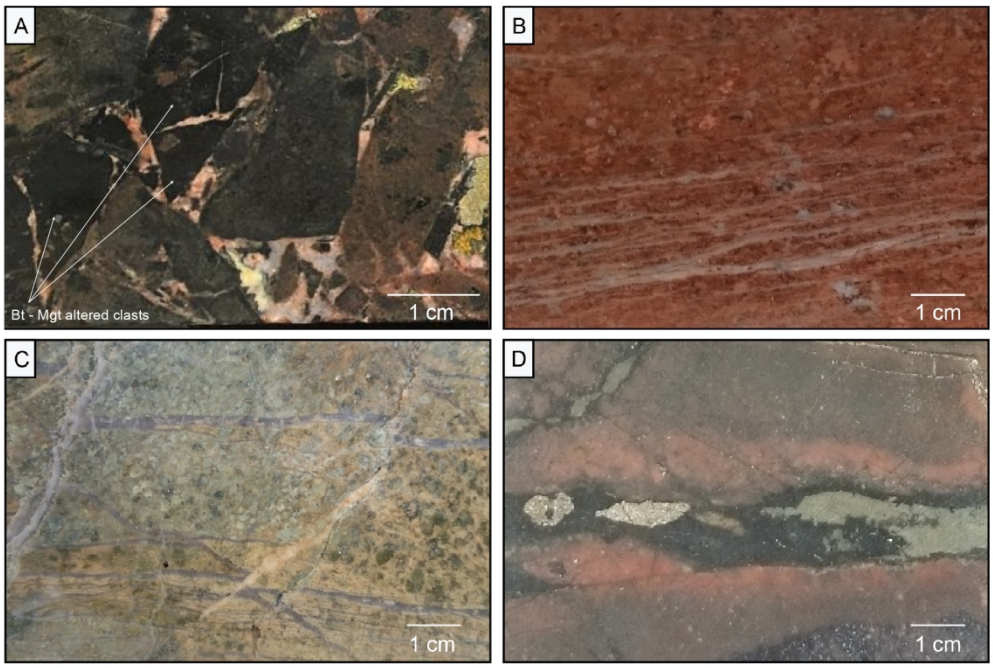

Figure 7: (a) biotite magnetite alteration in Two-Thirty breccia (b) sheeted quartz veins in KHB-QMP (c) altered KHB-QMP with sheeted veins and late carbonate crosscutting (d) magnetite-epidote-pyrite veins with K-feldspar selvages occur in the Goonumbla Volcanics in drillhole D245 at 810.96 m and in D247 at 461.72 m these rare occurrences are not observed within the Two-Thirty Breccia itself.

210x141mm (300 x 300 DPI)

Pre-brecciation alteration* - Stage 1					
Vein stage	**Host Lithology**	**Pre-breccia alteration**	**Vein mineral 1**	**Vein mineral 2**	**Alteration selvedge**
1A	Goonumbla sandstone	Biotite - magnetite	Pyrite	Chalcopyrite	Epidote
1B	Goonumbla siltstone	Biotite - magnetite	Quartz	Pyrite	Minor epidote
1C	Two-Thirty porphyry	K-Feldspar	Quartz	Molybdenum-pyrite - chalcopyrite	K-feldspar
Syn-brecciation alteration – Stage 2					
Breccia Facies	**Clast alteration**	**Matrix alteration**			
A1	Biotite-magnetite	none			
A2	Biotite-magnetite	none			
A3	Quartz-muscovite-phengite	Quartz altered where present			
C1	Biotite-magnetite	None			

** Stage 1D veins are omitted from this table as they may be pre- or syn-brecciation.*

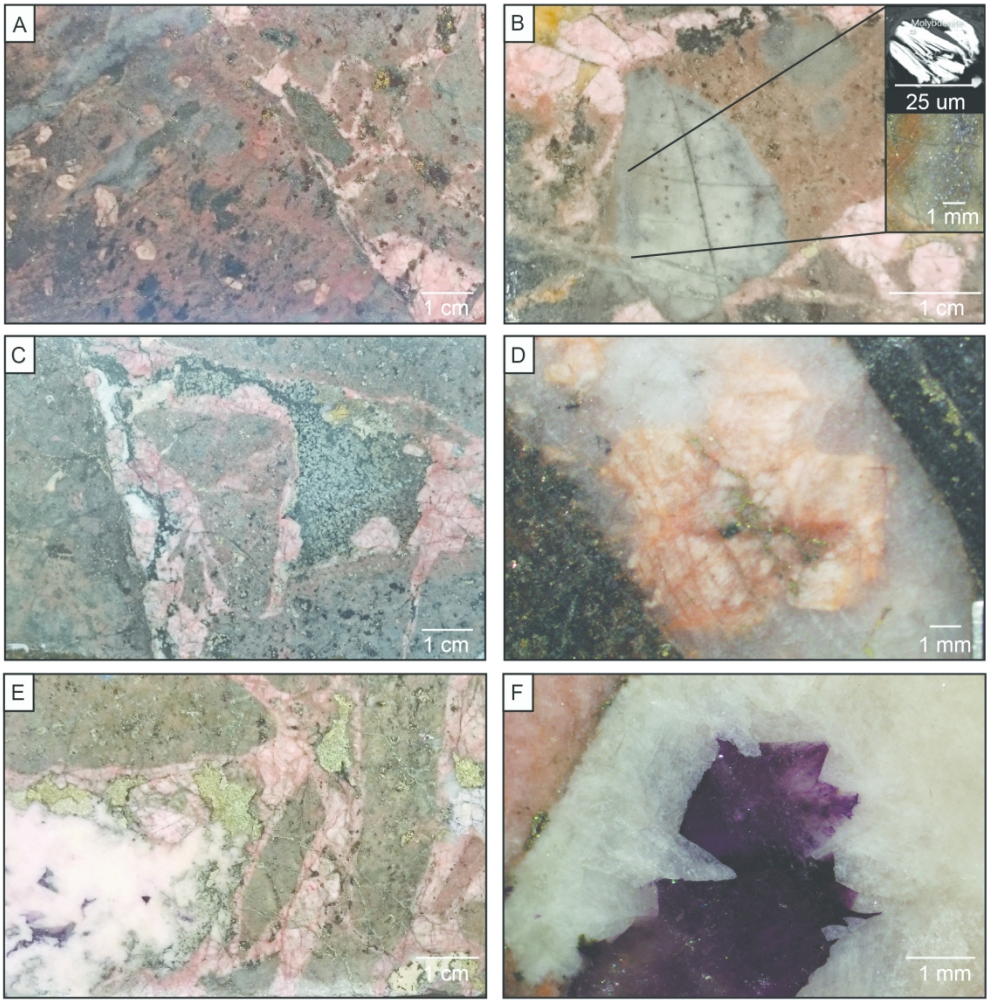

Figure 8: (a) Juvenile clast of the two-thirty porphyry in the A1 breccia facies. (b) Truncated quartz – molybdenite vein (c) K-feldspar cement with hematite dusting in the A1 breccia (d) brecciated early K-feldspar cement in a quartz vein (e) open space fill by late chalcopyrite + pyrite (f) Carbonate + fluorite cement phase in the A1 breccia.

185x188mm (300 x 300 DPI)

Table 6: Summary of ages obtained from the Two-Thirty intrusive complex and previous geochronology in the Northparkes district.

Sample Lithology	Sample Number	Mineral	Method	Age (Ma)		σ 1
Zero porphyry	NP16TW122	Zircon	U-Pb	438.8	±	4.4
				455.5	±	4.4
Altered K-QMP	NP16TW133	Zircon	U-Pb	447.1	±	4.5
Monzonite porphyry	NP16TW053	Zircon	U-Pb	447.3	±	4.5
Two-Thirty porphyry	NP16TW168	Zircon	U-Pb	448.0	±	4.5
KHB-QMP clast	NP16TW077	Zircon	U-Pb	450.5	±	4.5
Two-Thirty breccia	NP16TW079	Molybdenite	Re-Os (Mo)	438.9	±	1.4
Previous Geochronology at Northparkes						
Sample Lithology	**Sample Number**	**Mineral**	**Method**	**Age (Ma)**		**σ 1**
E26 Monzodiorite		Hornblende (p)	$^{40}Ar/^{39}Ar$	495.6	±	26.4
E26 BQM		Biotite (p)	$^{40}Ar/^{39}Ar$	437.3	±	2.1
E26 BQM		Zircon	U-Pb (SHRIMP)	444.2	±	4.7
E26 B-QMP late-min		Biotite (p)	$^{40}Ar/^{39}Ar$	446.5	±	2.6
E26 Alteration / min		Biotite (s)	$^{40}Ar/^{39}Ar$	441.3	±	3.8
E26 Alteration/ min		Sericite	$^{40}Ar/^{39}Ar$	439.2	±	1.2
E22 pre-min B-QMP		Biotite (p)	$^{40}Ar/^{39}Ar$	448.6	±	7.0
Wombin intrusion		Zircon	U-Pb (SHRIMP)	438.9	±	4.7
Wombin intrusion		Zircon	U-Pb (SHRIMP)	439.1	±	4.5
E37 zero porphyry		Zircon	U-Pb (SHRIMP)	436.7	±	3.3
Condoblin monzodiorite		Zircon	U-Pb (SHRIMP)	481.0	±	4.0

*** (p) denotes a primary phenocryst (s) denotes a secondary phase.**

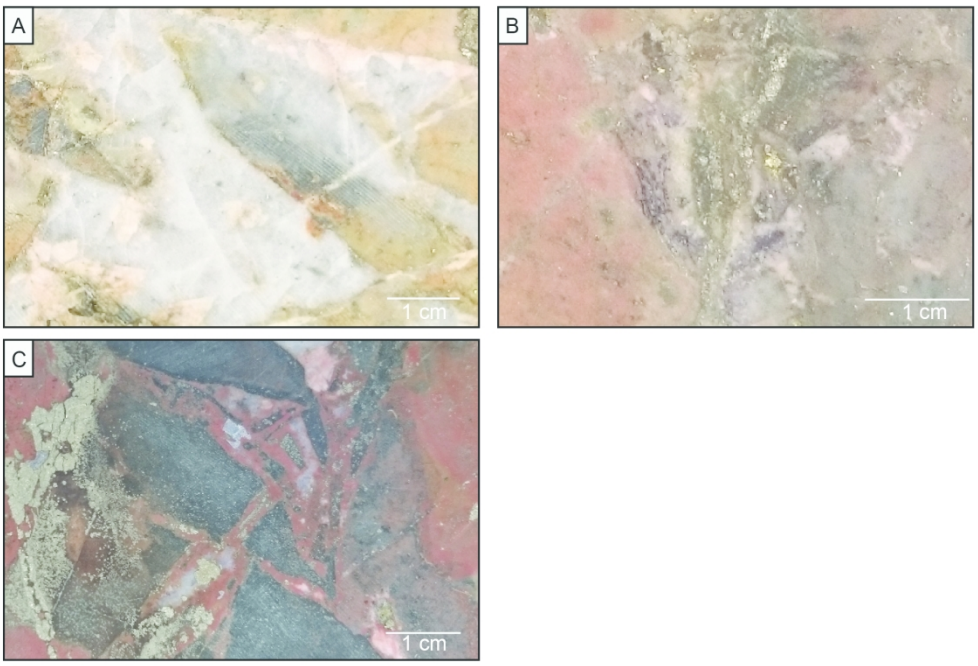

Figure 9: Two-Thirty breccia complex A2 and A3 Facies, (a) Quartz dominant cement with fractured earlier K-feldspar as cockade textures on clasts. (b) Fluorite bands with carbonate and brecciated k-feldspar infill (c) Igneous cement in the C1 breccia facies toward the base on the Two-Thirty breccia. This breccia facies is gradational to the A1 facies.

187x125mm (300 x 300 DPI)

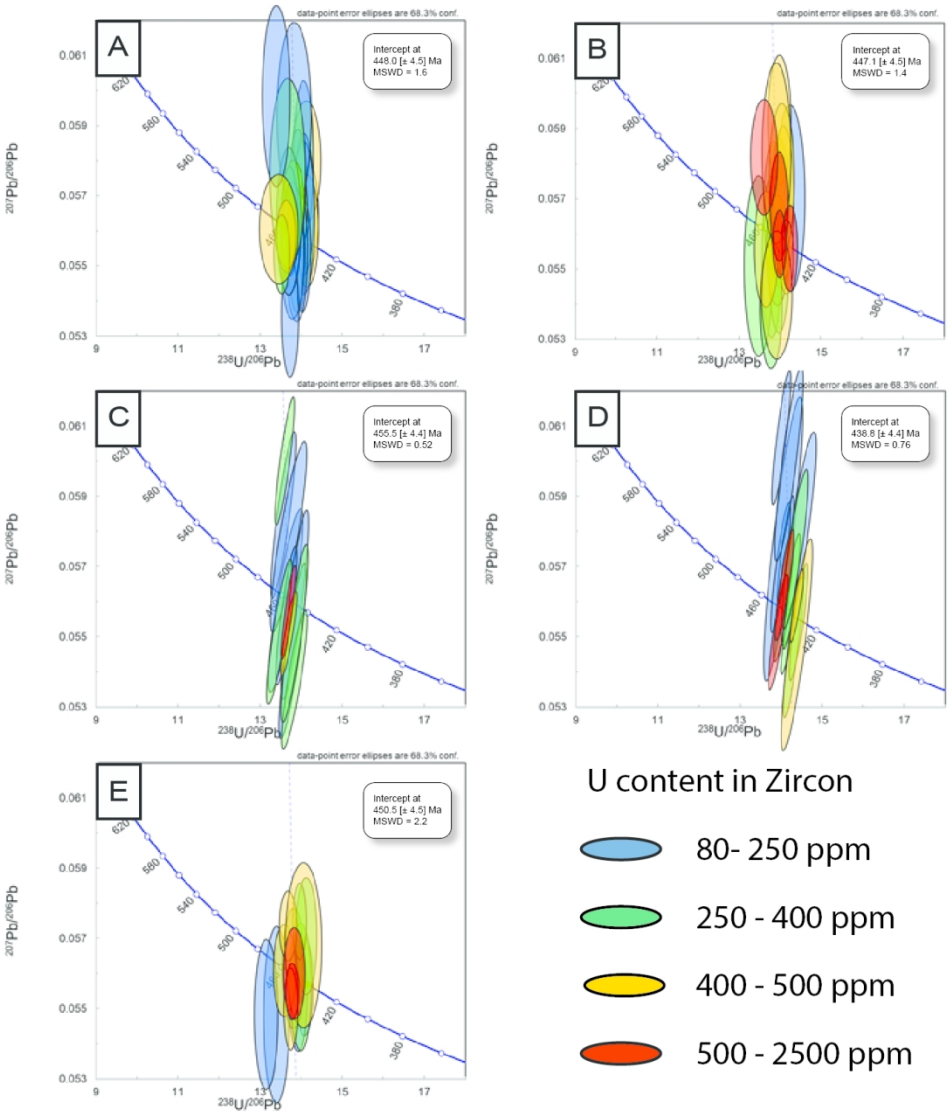

Figure 10: Zircon U-PB concordia diagrams for selected phases from the Two-Thirty intrusive complex, 2 σ error is represented by ellipse. Ellipse colour represents U content in zircons as an indicator of metamictisation (a) NP16TW168 the Two-Thirty porphyry (b) NP16TW133 Altered K-QMP (c) older of the two populations from the NP16TW122 zero porphyry sample (d) younger of the two populations from the zero porphyry (e) NP16TW053 monzonite sample (f) NP16TW077 KHB-QMP pre-mineralisation porphyry.

126x143mm (300 x 300 DPI)

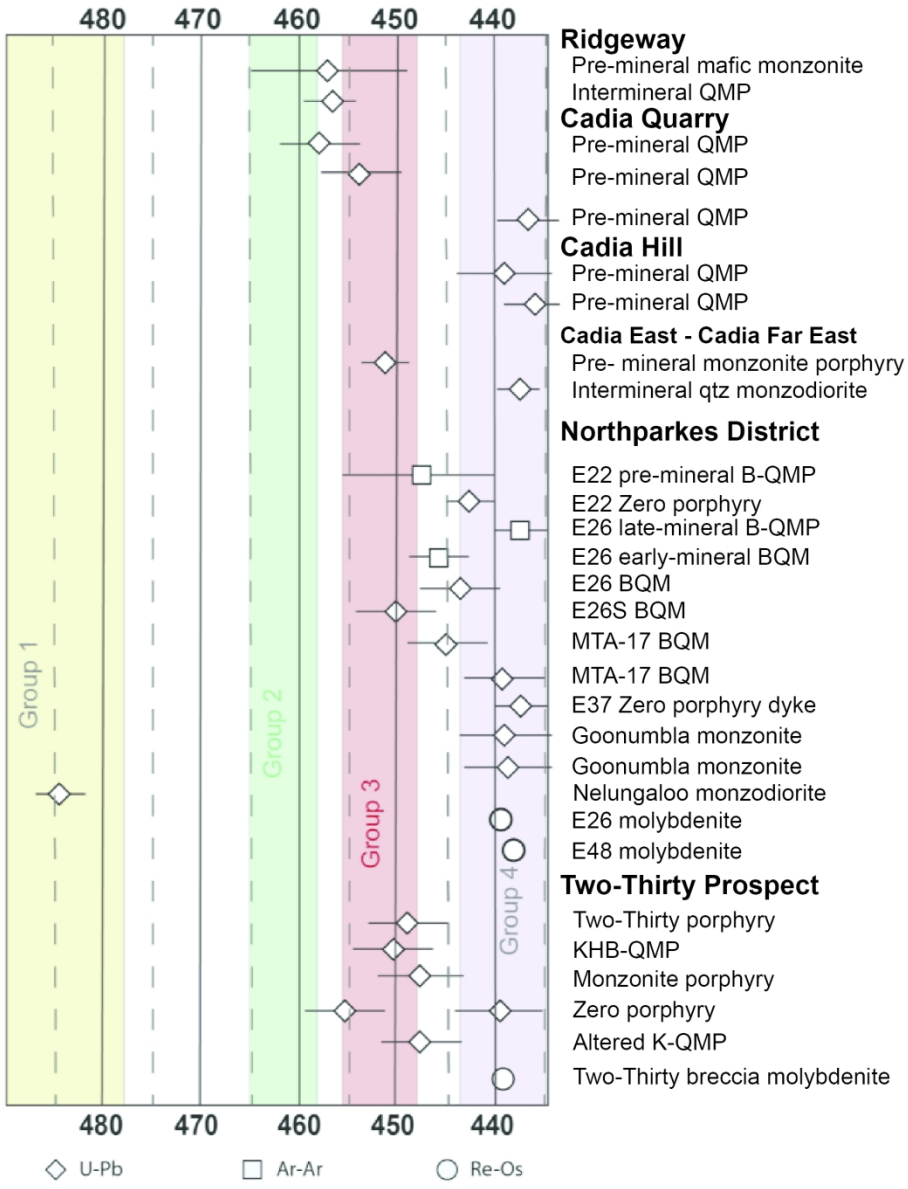

Figure 11: Two-Thirty intrusive complex in the context of regional geochronology, modified after Zukowski (2010); Rush, (2013). Abbreviation denote the following qtz – quartz, ccpy – chalcopyrite, cal – calcite, mlb – molybdenite.

175x221mm (300 x 300 DPI)

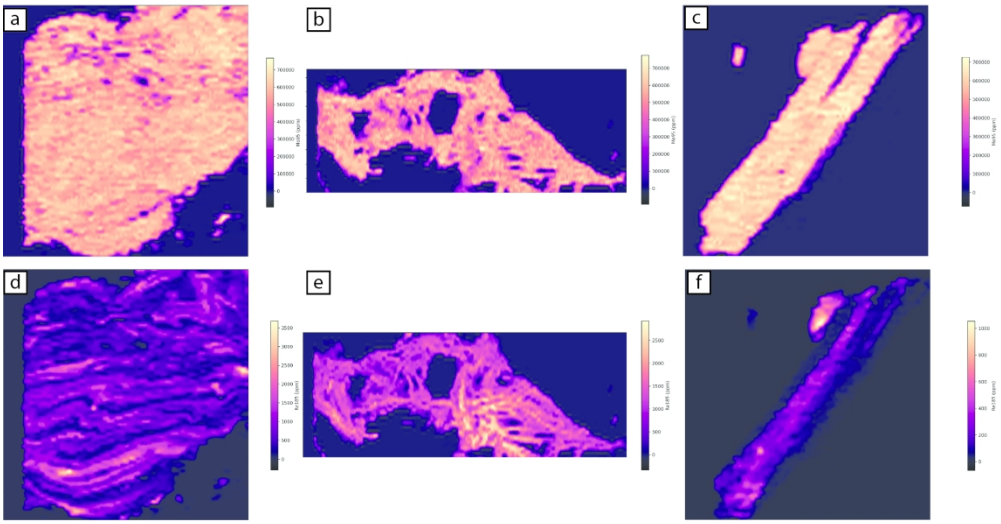

Figure 12: Distribution of Mo and Re in molybdenite grains from across the Northparkes district (a & d) NP17TW55 vein hosted molybdenite from E48 (b &e) vein hosted molybdenite from E27 (c & f) Molybdenite as a late infill mineral in the A3 magmatic-hydrothermal breccia facies at Two-Thirty. Re distribution in molybdenite from E48 and Two-Thirty varies by an order of magnitude. At E27 some variation is likely due to the fibrous habit of molybdenite and the lag between ablation and mass spectrometry which smears the response to the left, at Two-Thirty the variation occurs within a single filament of molybdenite with a high Re core and lower Re rim indicating a later hydrothermal molybdenite event. LA-ICPMS images are made on a left to right raster, lag time between ablation site and mass spectrometer is responsible for the 'shadowing/smearing' of the signal on the right side of each grain.

210x109mm (300 x 300 DPI)

Table 7: Re-Os dates from Molybdenite across the Northparkes district

Lithology	Deposit	Sample #	Age (Ma)	Error (2σ)	Re (ppm)
Vein hosted	E48	NP17TW055	437.6	2.2	1264.4
Vein hosted	E27	NP17TW048	439.0	2.2	1717.4
Two-Thirty breccia (A3 facies)	Two-Thirty	NP16TW079	438.9	2.2	224.60